ACS Catalysis

Review

pubs.acs.org/acscatalysis

Perovskite Oxides: Preparation, Characterizations, and Applications in Heterogeneous Catalysis

Junjiang Zhu,*[,†] Hailong Li,[†] Linyun Zhong,[†] Ping Xiao,[†] Xuelian Xu,[†] Xiangguang Yang,*[,‡] Zhen Zhao,*[,§] and Jinlin Li[†]

[†]Key Laboratory of Catalysis and Materials Science of the State Ethnic Affairs Commission & Ministry of Education, South-central University for Nationalities, 182 minzudadao, Wuhan 430074, China

[‡]State Key Laboratory of Rare Earth Resource Utilization, Changchun Institute of Applied Chemistry, Chinese Academy of Sciences, 5625 Renmin Street, Changchun 130022, China

[§]State Key Laboratory of Heavy Oil Processing, College of Science, China University of Petroleum, 18 Fuxue Road, Chang Ping, Beijing 102249, China

ABSTRACT: Perovskite oxides with formula ABO_3 or A_2BO_4 are a very important class of functional materials that exhibit a range of stoichiometries and crystal structures. Because of the structural features, they could accommodate around 90% of the metallic natural elements of the Periodic Table that stand solely or partially at the A and/or B positions without destroying the matrix structure, offering a way of correlating solid state chemistry to catalytic properties. Moreover, their high thermal and hydrothermal stability enable them suitable catalytic materials either for gas or solid reactions carried out at high temperatures, or liquid reactions carried out at low temperatures. In this review, we addressed the preparation, characterization, and application of perovskite oxides in heterogeneous catalysis. Preparation is an important issue in catalysis by which materials with desired textural structure and physicochemical property could be achieved; characterization is the way to explore and understand the textural structures and physicochemical properties of the material; however, application reflects how and where the material could be used and what it can solve in practice, which is the ultimate goal of catalysis. This review is organized in five sections: (1) a brief introduction to perovskite oxides, (2) preparation of perovskite oxides with different textural structures and surface morphologies, (3) general characterizations applied to perovskite oxides, (4) application of perovskite oxides in heterogeneous catalysis, and (5) conclusions and perspectives. We expected that the overview on these achievements could lead to research on the nature of catalytic performances of perovskite oxides and finally commercialization of them for industrial use.

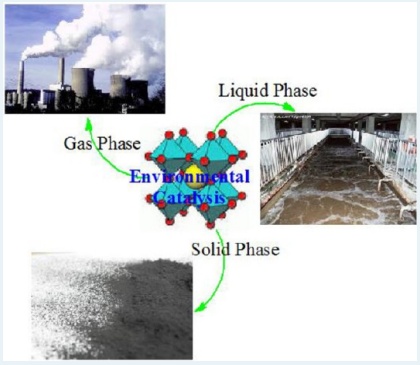

KEYWORDS: *perovskite oxide, preparation, surface morphology, characterizations, catalysis*

1. INTRODUCTION

Perovskite, originated from $CaTiO_3$, is now a general name for oxides having the structural formula ABO_3 or A_2BO_4. In the ABO_3 structure, the A-site cation is 12-fold coordinated and the B-site cation is 6-fold coordinated with oxygen anions, as simply depicted in Figure 1.[1] The A_2BO_4 oxides are composed of alternated ABO_3 and AO layers, and they are sometimes called perovskite-like oxides. For simplicity, both ABO_3 and A_2BO_4 oxides are uniformly named as perovskite in this review. In the framework, A is a larger cation located on the edge of the structure, and B is a smaller cation located in the center of the octahedron, with the lowest limits for cationic radii of $r_A > 0.09$ nm and $r_B > 0.051$ nm.

The material has high structural stability, and the A- and/or B-site cation can be substituted by a foreign cation having different oxidation state or radius,[2−4] thus the oxidation state of B-site cation and the content of oxygen vacancy can be controlled when desired foreign cation is used, offering a convenient and feasible way of correlating physicochemical properties with catalytic performances of the materials.

The degree of substitution at the A- and/or B-site cation however is not liberal, as this would lead to deviation of framework and finally destroy the matrix structure. All the cations in the structure should meet the restriction of $0.75 < t < 1.0$, where $t = (r_A + r_O)/\{\sqrt{2}(r_B + r_O)\}$ is the tolerance factor of perovskite oxides, and r_A, r_B, and r_O are the radii of the respective ions.[5]

From the composition, it can be seen that perovskite oxides are compounds consisting of two or more simple oxides having high melting point. Thus, the preparation of pure perovskite oxides or the integration of metal oxides should be conducted at high temperature with long calcination time, leading to low surface area. Perovskite thus prepared showed low efficiency in

Received: January 3, 2014
Revised: July 17, 2014
Published: July 17, 2014

   dx.doi.org/10.1021/cs500606g | ACS Catal. 2014, 4, 2917−2940

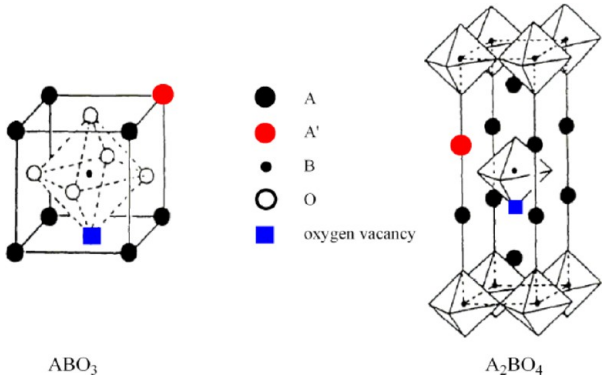

Figure 1. Ideal models of perovskite oxides with ABO_3 and A_2BO_4 structure. The red dot represents the substitution of an A-site cation by a foreign one; the blue square represents the oxygen vacancies. The oxygen symbol is not shown in the A_2BO_4 structure for simplification.[1]

surface catalyzed reactions, which require high surface area for contact of the substrate. In order to lower the calcination temperature and increase the surface area, many efforts[6−10] have been paid to improve the preparation method or to synthesize the material with different textural structures. The traditional strategy by simply adding organic complexing agent to combust the precursor seems inefficient in this aspect. For instance, $LaCoO_3$ prepared by citric combustion method and calcining at 800 °C for 6 h showed a surface area of only 9 m^2/g.[11] The more desirable way of improving the surface area is to prepare small-dimension or porous perovskite oxides with different surface morphologies, which had been proven successful in the recent years.

Characterizations are essential in understanding the structures and properties of the perovskite oxides synthesized. The differences in crystal and/or textural structure would certainly lead to variation in the properties, and for better understanding, the samples should be synthesized with pure phase and defined crystalline. In characterizing the crystal and textural structures of perovskite oxides conventional measurements like XRD, FT-IR, DSC/DTA-TG, N_2 physisorption isotherms, TEM, and SEM are usually used. In some cases, for example, the detection of Pd incorporation in the perovskite, EXAFS is also conducted to reveal the actual status of Pd in the structure.[12−14] As for the measurements used for characterizing the physicochemical properties, temperature-programmed desorption of oxygen (O_2-TPD), temperature-programmed reduction of hydrogen (H_2-TPR), and X-ray photoelectron spectroscopy (XPS) are normally indispensable, as they could provide information on the oxygen vacancy, the reducibility and the binding energy (or the oxidation state) of metal and oxygen elements of the perovskite oxides, which are important properties resulted from the structure features. There are certainly many other important measurements, such as the oxygen storage (complete) capacity (OSC/OSCC) and the redox potentials, which also provide useful information on the properties of perovskite oxides. With suitable characterizations, deep insight into the structure of the material and intrinsic factors which determine the reaction in question could be obtained, which in turn would direct us to synthesize more efficient catalyst for the reactions.

Application of perovskite oxides to heterogeneous catalysis can be traced back to 1952 and 1953 by Parravano, who reported the catalytic performances of $NaNbO_3$, $KNbO_3$, and $LaFeO_3$ for CO oxidation.[15,16] Since then, a great deal of research using perovskite oxides as catalyst for heterogeneous reactions has emerged. Because of the structural features like high thermal and hydrothermal stability, perovskite oxides can be applied to various types of reactions, either gas or solid reactions conducted at high temperature or liquid reactions conducted at room temperature, and even those conducted under irradiation conditions.[17−20] Although perovskite oxides have not yet been applied in industry up to date and there is still a long way to walk on before their commercialization, their easy availability, wide applicability, and especially controllable physicochemical properties enable them energetic materials for investigation in catalysis.

This review summarized the methods for the preparation of perovskite oxides with different surface morphologies, introduced the conventional measurements used for their characterization, and examined their application in several typical reactions in catalysis. Although there have many review articles giving deep insight into the structure and catalytic performances of perovskite oxides,[2,3,21−26] this review attempted to provide basic knowledge on the synthesis, characterizations, and applications of perovskite oxides in catalysis.

2. SYNTHESIS OF PEROVSKITE OXIDES WITH DIFFERENT MORPHOLOGIES

2.1. Synthesis of Bulk Perovskite Oxides. The synthesis of bulk perovskite oxides in principle is simple, which can be conducted by direct annealing of the mixture of corresponding metal oxides at high temperatures.[27−29] This method is environmentally friendly as the product is synthesized directly from the metal oxides without releasing toxic gas. However, it is essential to homogenize the metal oxide precursors so that they can react with each other thoroughly and form pure pervoskite oxides. In this respect, the mixture could be treated by ball mill[30] or by stabilized ZrO_2 balls in ethanol.[31] Such prepared sample has low surface area and large particle size, and is usually applied to, for example, the field of ceramics that requires good mechanical property.[32,33]

In order to be applied in catalysis, the increase of surface area and/or the decrease of particle size of the perovskite oxides are essential because catalysis belongs to a class of surface reaction that requires good contact between the substrate and the catalyst's surface. The preparation of perovskite oxides with high surface area thus is desired. One efficient way is to use soluble metal nitrates, instead of metal oxides, as the precursors and the preparation is conducted in the presence of organic complex, which is used to coordinate, combust, and disperse the metal oxide particles. For example, in the citric acid combustion method, metal nitrates are usually used as precursors, and citric acid is used as organic complex to coordinate metal ions.[34−36] After undergoing a dissolution and combustion process, small and homogenized metal oxides particles, which are the precursors of perovskite oxides, can be obtained. This allows the subsequent formation process conducted at low temperature range (700−900 °C) with short calcination time (2−5 h), resulting in improved surface area (relative to that prepared by direct annealing method). Although the surface area of perovskite oxide prepared by citric acid combustion is still not highly satisfactory,[37] this method is widely adopted to prepare perovskite catalysts in catalysis even today, because of the simple operation process as well as the considerable catalytic performances.

It should be noted that because of the presence of nitrates and organic complexes, unwanted gases such as NO_2 and CO_2

dx.doi.org/10.1021/cs500606g | ACS Catal. 2014, 4, 2917−2940

will be released during the process, and thus the preparation should be carried out in a fuming cupboard or at a place where the air can be well ventilated. Also it has to be mentioned that the formation of carbonates (e.g., $SrCO_3$)[38] is inevitable as the organic complex can be a carbon resource. The presence of carbonates may influence the catalytic performances of the material in some reactions, and its amount should be minimized as far as possible.

2.2. Synthesis of Nanosized Perovskite Oxides. One efficient way of decreasing the particle size of perovskite oxides is to synthesize them on a high-surface-area support such as mesoporous silica,[39−42] Ce−Zr−O,[43] MgO,[44] Al_2O_3,[45] among others, on which the particles can be highly dispersed and their aggregation is hindered, leading to nanosized particles. In this method, the precursors should be soluble salts so that they can be dissolved and late homogeneously impregnated on the support's surface, and the support should be surface inactive in order to avoid reacting with the precursors and entering into the lattice of perovskite oxides.[46] If necessary, coating of precursors (e.g., La_2O_3 on Al_2O_3) on the surface of the support is required, to prevent the support from incorporating into the perovskite's framework.[47−49]

Supported perovskite oxides can be prepared by an impregnation method. The desired metal salts were first mixed and dissolved in an aqueous solution, and after complete dissolution the desired support was added. The mixture was then heated at certain temperature (e.g., 80 °C) with vigorous stirring in order to remove the water and deposit the metal ions homogeneously on the support. Organic complex can be added in this step to chelate the metal ions,[50] to yield better-dispersed and fine metal oxides powders, which are intermediates in the formation of perovskite oxides. The obtained sample was finally calcined at setting temperature (e.g., 700 °C), to yield the product.

As a common advantage of the impregnation method, the loading of perovskite oxides can be controlled by calculating the mass of precursors at the weighing step. Because of the support effect, the temperature required for the formation of perovskite oxides could be lowered, and their physicochemical properties could be altered due to an interaction with support. The measurement of surface area of supported perovskite oxides however is a problem, as it is not possible to differentiate the contribution from the support, and therefore, the surface area obtained from N_2 physisorption isotherms is not for the real perovskite oxides but for the perovskite-support composite. The chemisorption method that is normally used to measure the surface area of supported noble metal nanoparticles (e.g., Pt) is ineffective in this case. In addition to the impregnation method, supported perovskite oxides can also be prepared by many other methods, including coprecipitation,[51,52] coating,[53,54] in situ preparation,[55] and deposition−precipitation.[49,56]

As expected, the particle size of perovskite oxides can be largely decreased when prepared on a support, Figure 2, and it can be expected that smaller particles can be obtained when the loading of the material was decreased by decreasing the concentration of the precursors. The formation of perovskite particles both on the surface and inside the pores of support is possible as the aqueous precursors could permeate into the pores, but the former is the majority. Small particle size can on one hand improve the exposure and the utilization of active site, and on the other hand, they interact strongly with the support, altering the physicochemical properties and leading to enhanced surface properties.

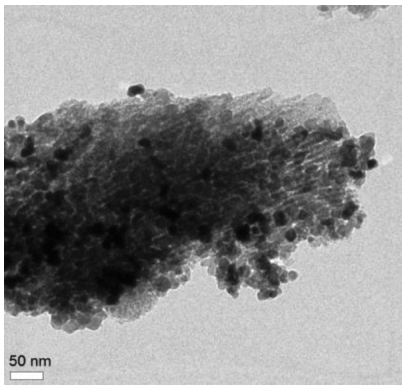

Figure 2. TEM image for supported $LaFeO_3$/SBA-15, where the black spots are $LaFeO_3$.[41]

Besides the supporting strategy, mechano-synthesis is also an effective way of synthesizing nanosized perovskite oxides.[57−61] In this method, the corresponding metal oxides were mixed and reacted with each other in a high-energy ball milling reactor. The energy required for the reaction is provided by the collision of the high-speeding balls in the reactor and no heat from external is needed. This method is easy to operate, and no toxic gas will be released, but the reaction conditions are highly vigorous (e.g., agitation speed of 1100 rpm for 20 h[62]), and thus the requirement for the equipment is critical and the operation should be very careful. Kaliaguine et al. have reported that nanosized perovskite prepared by this method (reactive grinding) are good catalysts for certain reactions including VOC oxidation and NO reduction.[62−65] To lower the demands for the equipment, Zhang et al. suggested to synthesize bulk perovskite oxides first, which was then grinded by a ball milling reactor to decrease the particle size. This was proved to be effective in promoting the catalytic activity of the material in, for example, C_3H_6 SCR NO reaction.[66] The reaction mechanism as well as the influence of reaction conditions (e.g., the ball types, the powder-to-ball mass ratio, the reaction atmosphere) on the properties of the material has been well documented recently by Perez-Maqueda et al.[67]

2.3. Synthesis of Porous Perovskite Oxides. Although the decrease in particle size could enhance the ratio of surface to bulk atoms and the contact area for the reactant, the surface area and the utilization of surface of nanosized perovskite oxides is still below expectation. Further, as the nanoparticle does not have pores, this makes the reaction occur only on the external surface, limiting the catalytic capacity of the material. This is especially pronounced when the material is applied to reactions involving solid reactant.[7] To this end, the use of porous perovskite oxides would be helpful, as porous material could allow the adsorption of reactant on both the surface and inside the pores, improving the contact area and thus catalytic performances.[68,69] However, porous materials have weaker mechanical strength than the bulk, and the pores could be collapsed if severe conditions are used. This has to be considered before the reaction.

The synthesis of porous perovskite oxides is often conducted by a template method using either hard or soft templates. Depending on the template, perovskite oxides with different textural structures could be prepared. In that case of a hard template (also known as nanocasting method), porous silicas, because of their miscellaneous structures, are regarded as a promising template and have been received great attention over

the years.[9,70] For instance, Lu et al. reported that mesoporous $LaCoO_3$ can be replicated using vinyl grafted SBA-15 as a template.[70] In the process, an equimolar ratio of lanthanum and cobalt nitrates were first dissolved in a water−ethanol solution containing citric acid, whose amount equals to the total moles of lanthanum and cobalt. To this solution, the preprepared SBA-15 template was added. The mixture was stirred at 40 °C until it became viscous, which was then dried at 80 °C for 6 h, calcined at 500 °C for 4 h and 700 °C for another 4 h (ramp, 2 deg/min). The obtained sample was finally treated in 2 M NaOH aqueous solution at room temperature to etch the silica framework and yield the porous $LaCoO_3$, see Figure 3A.

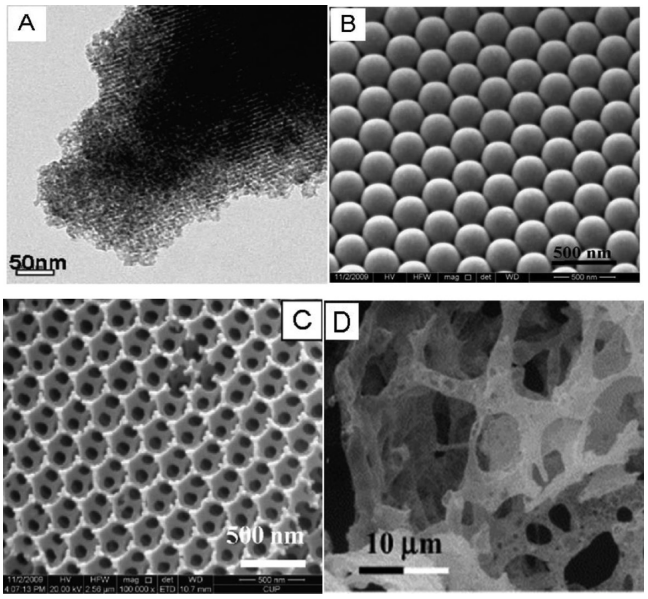

Figure 3. (A) TEM image for mesoporous $LaCoO_3$;[70] (B) SEM image for monodisperse PMMA microspheres;[7] (C) TEM image for 3-DOM $LaFeO_3$;[7] and (D) SEM image for $LaMnO_3$.[71]

The use of polymeric material as a soft template for the preparation of porous perovskite oxides has also received great interest recently.[7,72−76] Zhao et al. reported that poly(methyl methacrylate) (PMMA) microspheres are good template for the preparation of three dimensionally ordered macroporous (3DOM) perovskites $LaCo_xFe_{1-x}O_3$. They first prepared non-cross-linked, monodisperse PMMA microspheres (Figure 3B), which was then added to a ethylene glycol (EG)−methanol solution containing desired metal nitrates (e.g., La^{3+}, Co^{2+}, Fe^{3+}). The resulting mixture was subsequently dried and calcined at setting temperature to yield the 3-DOM perovskite oxides (see Figure 3C).[7]

In general, the soft template is preferred to the hard one for preparing porous inorganic oxides, as the former can be simply and fully removed during the calcination process, and the creation of pores as well as the formation of desired oxides can proceed at the same time. In comparison, the removal of hard template requires extra or post-treatment steps before obtaining the target product. For example, in the preparation of porous $LaCoO_3$ using silica as template, the calcined $LaCoO_3$-silica composite needs to be treated in NaOH solution before obtaining the final product. Furthermore, residue silica in the final product is possible, which may contaminate and interfere with the catalytic behaviors of the product, and further, the oxides' structure could be destroyed during the treatment process due to the drastic conditions used.

However, the preparation of soft template with controlled properties in most cases is more complex and difficult than that of hard template. For the PMMA and SBA-15 mentioned above, the preparation and separation of 3-DOM PMMA from the solution is difficult because of the low density of PMMA, thus the separation process (by centrifugal machine) needs high rotational speed and long rotational time. In addition, the formation of PMMA is sensitive to the environmental conditions and randomly arranged PMMA is usually yielded.[76] In contrast, the ordered mesoporous SBA-15[77−79] can be simply separated, and large-scale synthesis is possible under mild conditions.

Besides the template method, solution combustion synthesis (SCS) has also been reported to be an effective method for the preparation of porous perovskite oxides, with surface area up to 60 $m^2\ g^{-1}$.[80−83] This method has the advantages of exothermic, fast, and self-sustaining chemical reactions between metal salts and a suitable organic fuel, thus the heat in the synthesis can be supplied mostly by the reaction itself.[71] Furthermore, the precursors and the fuel can be cheap materials, and the operation is simple, making it a feasible method for large-scale preparation. The pore structure and size however is hard to control, and the pores are generally randomly distributed.

Scheme 1. Sequential Schematic Diagrams for the Preparation of LCMO Nanospheres by a Template-Assisted Method[87]

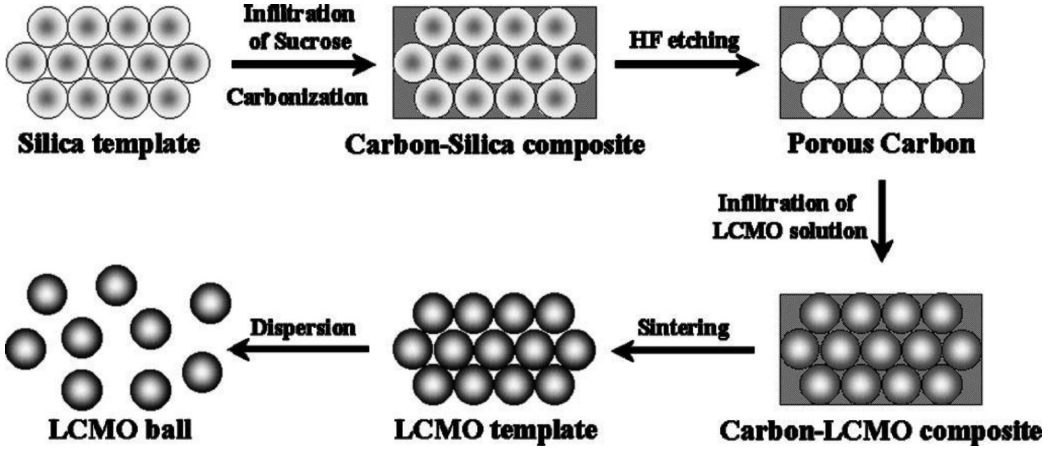

dx.doi.org/10.1021/cs500606g | ACS Catal. 2014, 4, 2917−2940

In the method, the precursors, normally soluble metal nitrates, and the fuels (e.g., urea) were first dissolved in an aqueous solution. After stirring for several minutes until homogeneity, the solution was transferred to a ceramic dish, which was placed into an oven preheated and kept at a constant temperature in the range of 400−800 °C. Depending on the temperature and the fuels used, materials with various morphologies can be obtained. Figure 3D depicted a SEM image of $LaMnO_3$ perovskite prepared by the CSC method using urea as fuel, showing obviously a porous structure.[71]

2.4. Synthesis of Hollow Nanospheres Perovskite Oxides. Hollow nanospheres perovskite also possesses enhanced surface area and surface energy relative to the bulk one due to the hollow structure, which provided a double face (inner and external) to contact with reactants. Thus, improved catalytic performances could be expected on such perovskite oxides. In the preparation of hollow perovskite, two strategies are usually adopted: one is to use spherical template such as carbon spheres to replicate the material,[84] and the other is to use organic directing agents and by a hydrothermal process, to synthesize the hollow material directly.[85,86] Detailed preparation processes of the two strategies are described below.

In the first strategy, the carbon spheres could be prepared either by hydrothermal treatment of organic precursors (e.g., glucose) or by replication method using silica as template and then used as (secondary) template to replicate the hollow perovskite oxides. Scheme 1 illustrates the use of silica templated carbon spheres as a secondary template to synthesize hollow perovskite oxides.[87] Sucrose was first infiltrated into the silica template and then carbonized to form a carbon−silica composite, which was subsequently etched in an aqueous 48% HF solution to remove the silica template and yield the carbon replica. After that, a preprepared solution containing the desired metal cations were dropped into the carbon replica until the pores were completely filled with the solution. The resulting mixture was finally dried and calcined at setting temperature to yield the target product. The hollow status of perovskite oxides was confirmed by SEM and TEM image in Figure 4A.

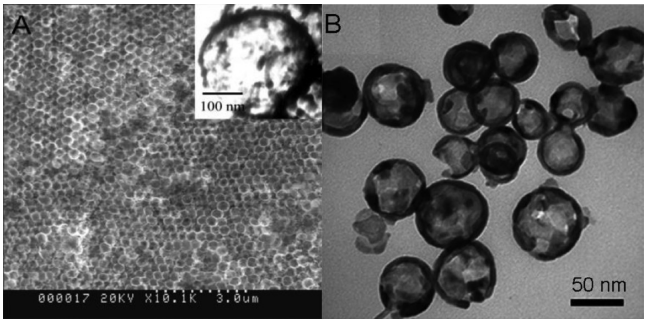

Figure 4. (A) SEM image of the $La_{0.7}Ca_{0.3}MnO_3$ sphere array replicated from the carbon template. The inset is a TEM image of a $La_{0.7}Ca_{0.3}MnO_3$ sphere, exhibiting a hollow sphere feature;[87] (B) TEM image of $LaMnO_3$ prepared by hydrothermal method.[86]

For the hydrothermal method, a brief process reported by Zhang et al.[86] is described as below. The desired amounts of metal nitrates, citric acid, urea and P123 were first dissolved in a solution containing ethanol, ethylene glycol, and water. After complete dissolution, the solution was transferred into a stainless autoclave and heated at 100 °C for 48 h. The resulting solid product was then centrifuged and dried, and finally calcined at 600 °C for 8 h in an air flow to yield the perovskite oxide, and the hollow status was well-supported by the TEM image in Figure 4B.

By comparison, in the carbon spheres template route, the preparation of carbon spheres has to be completed before synthesizing the hollow perovskite oxide, which makes the overall procedures complex. Because the silica template has uniform particle size, the carbon spheres and later the perovskite oxides with uniform particle size can be replicated. Furthermore, the particle size of perovskite oxides can be controlled by selecting silica with desired particle size. In the hydrothermal route, the procedure for preparing hollow perovskite oxide is relatively simple, but the particle size and shape of the resulting perovskite oxide is hard to control because the condensation process of organic directing agents is uncontrollable, which may affect the properties and catalytic performances of the material.

2.5. Synthesis of Other Morphological Perovskite Oxides. With the development of materials science and the increasing demand for special use, perovskite oxides with various morphologies have been synthesized, including nanoplate,[88,89] nanofibers,[90,91] nanotubes,[92,93] flower-like,[94] and cubic.[95−97] These different morphologies would enable the perovskite oxides to possess rich surface properties and widen their applications. In this review, however, we do not attempt to describe the detailed preparation process for all these perovskite oxides, and for additional details, we would like to refer the reader to the literature listed above.

3. CHARACTERIZATIONS

3.1. Crystal and Textural Structure. Identification of crystal structure is the necessary and primary step before applying a material for investigation. For inorganic materials including perovskite, XRD is one of the simplest measurements to identify the crystal structure, which can be confirmed by comparing with the standard database of powder diffraction file (PDF). Rietveld refinement based on XRD data can further be applied to calculate the unit cell parameters and identify the deviation from the ideal structure. Besides XRD, FT-IR and EXAFS are also useful and widely used in determining the crystal structure of material. The FT-IR spectrum shows two characteristic absorption bands at near 600 and 400 cm^{-1}, which are attributed to the stretching and bending vibrations of B−O bond of ABO_3-type perovskite, respectively,[98] whereas the EXAFS spectrum could provide detailed information on the coordination environment of a metal, identifying whether it is in a perovskite environment. This is especially useful when the metal incorporated into the perovskite structure is in a small amount, which exceeds the detection limit of XRD measurement.

For the textural properties, N_2 physisorption is a powerful means, which provides direct information on surface area and pore structure of a material. As indicated above, catalysis belongs to a type of surface reactions, which implies that the reactants should be adsorbed and activated on the catalyst's surface before reacting with each other. Hence, the measurement of surface area is essential in discussing the catalytic performances of catalysts including perovskite oxides. As for the pore structure, it is usually measured when the perovskite was fabricated in porous status, to indicate how big the pore size is and in which form it exists. Besides the N_2 physisorption, SEM and TEM are also usually conducted, with the aim to check the

dx.doi.org/10.1021/cs500606g | ACS Catal. 2014, 4, 2917−2940

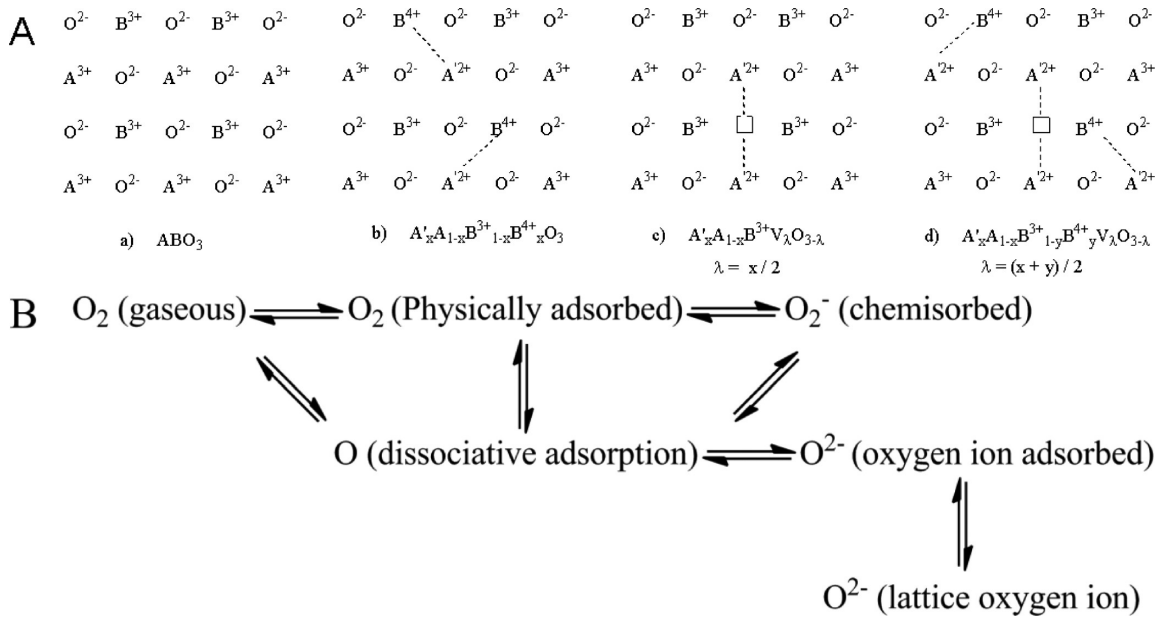

Figure 5. (A) Change in the oxidation state of B-site cation and the generation of oxygen vacancy in the defect $A^{3+}_{1-x}A'^{2+}_{x}BO_3$ structure. (B) Transformation of different oxygen species in the perovskite oxides with oxygen defects.[99]

surface morphologies, and in some cases to measure the particle size of the material. The various morphologies of perovskite oxides mentioned in section 2 were confirmed by the TEM images.

3.2. Transformation of B-Site Cation and Oxygen Species by Substitution. From the structural features of perovskite oxides, it is known that the oxidation state of B-site cation as well as the oxygen vacancy generated in the structure can be controlled by substitution with an external cation without destroying the matrix structure. Figure 5A presents a detailed description on the process based on a ABO_3-type perovskite,[99] showing that the oxidation state of B-site cation can be raised ($B^{3+} \rightarrow B^{4+}$) or the oxygen vacancy can be generated when A^{3+} cation is replaced by a A'^{2+} one in the $A^{3+}_{1-x}A'^{2+}_{x}BO_3$ structure. The control of the oxidation state of B-site metal cation and the number of oxygen vacancy is of great importance, as the catalytic cycle depends intimately on the redox properties of B-site metal cation, whereas oxygen vacancy provides the sites for substrate adsorption and activation. The oxidation state of B-site metal cation can be titrated by an iodometric method,[100−102] and the relationship between the number of oxygen vacancy generated and the oxidation state of B-site metal cation increased can be defined in theory according to the principle of electroneutrality. However, it should be noted that for the iodometric method, only one metal, with variable valences, could be presented in the catalyst, otherwise the calculation is not possible.

The increase of oxidation state of B-site metal cation or the generation of oxygen vacancy by substitution suggests that there exists an equilibrium in B^{4+}-(O^{2-})-B^{4+} = B^{3+}-□-B^{3+} + 1/2O_2 ("□" represents oxygen vacancy). That is, oxygen vacancy can be generated by losing one lattice oxygen, or vice versa, molecular oxygen can be adsorbed and activated (by receiving electrons) on the oxygen vacancy and subsequently be transformed into chemically reactive oxygen species. This implies that oxygen vacancy should be a bridge for the transformation of molecular and lattice oxygen. Wu et al. have illustrated an exhaustive transformation process between the various oxygen species occurring on oxygen-defected perovskite oxides, Figure 5B, showing oxygen vacancy acting as a bridge linking the molecular and atomic oxygen.

3.3. Temperature-Programmed Desorption of Oxygen. As demonstrated above, different oxygen species can be generated/transformed over perovskite oxides with oxygen vacancy, and these oxygen species should play a crucial role for reactions involving oxygen-containing species. To determine the quantity and the strength of these oxygen species on the surface thus is essential in understanding the catalytic performances of perovskite oxides. In this respect, temperature-programmed desorption of oxygen (O_2-TPD) is an effective technique, which gives simple and rapid analysis on the quantitative coverage and bonding strength information on oxygen species on the catalyst.

The conventional procedure of the O_2-TPD experiment for perovskite oxides is as below: the sample was first loaded in a fix-bed reactor and treated in oxygen atmosphere at certain temperature (e.g., 600 °C) for some time, and then cooled down in the same atmosphere to absorb the oxygen. Thereafter the carrying gas (e.g., helium) was switched on to remove the residue oxygen and stabilize the apparatus. After a stable baseline was obtained, the sample was heated again to a desired temperature (e.g., 800 °C), and the TPD profile was recorded by a thermal conductivity detector (TCD).

On the basis of the oxygen transformation process shown in Figure 5, four types of oxygen species could be involved in the O_2-TPD spectra, attributed to physical adsorption oxygen (O_2), ordinarily chemical adsorbed oxygen (O_2^-), oxygen adsorbed on oxygen vacancies (O^-), and lattice oxygen (O^{2-}). However, the physically adsorbed oxygen are hard to be detected in the measurement as it will be flushed away during the gas purging (or baseline stabilizing) process because of the weak interaction with the catalyst's surface. The ordinarily chemical adsorbed oxygen (O_2^-) also has weak interaction to the catalyst's surface and is rarely observed in ABO_3-type perovskite oxides,[103−107] but it can be detected in most A_2BO_4-type perovskite oxides. According to the literature, this oxygen species is desorbed at

dx.doi.org/10.1021/cs500606g | ACS Catal. 2014, 4, 2917−2940

temperature in the range of 60−300 °C.[108−111] The dissociative oxygen on oxygen vacancy is one of the most important properties of perovskite oxides, as it is involved directly in the reaction. The desorption of this oxygen species reflects not only the number of oxygen vacancy (active site) generated in the catalyst but also the difficulty of regenerating oxygen vacancy, thus the properties of this oxygen species is usually correlated to the catalytic performances. The desorption temperature for this oxygen species is in the range of 300−700 °C and has intimate relation to the nature of the B-site metal cation and the number of oxygen vacancy generated. The lattice oxygen, as its name implies, is the oxygen situated in the lattice of perovskite oxides and is the bridge linking the metal cations at the A- and B-sites. The desorption of lattice oxygen would lead to an increase in the oxidation state of B-site cation (assuming that the valence of A-site cation is unchangeable) according to the principle of electroneutrality, thus it is strictly related to the redox ability of the B-site cation.[104,105] The desorption of lattice oxygen usually occurs at temperature higher than 700 °C because of the high bond energy of B−O bond, which is also the origin of oxygen vacancy generated in the structure.

Figure 6A shows a typical O_2-TPD profile of $La_{1-x}Sr_xCoO_3$-based perovskite oxides.[112] The peak at temperature below 300

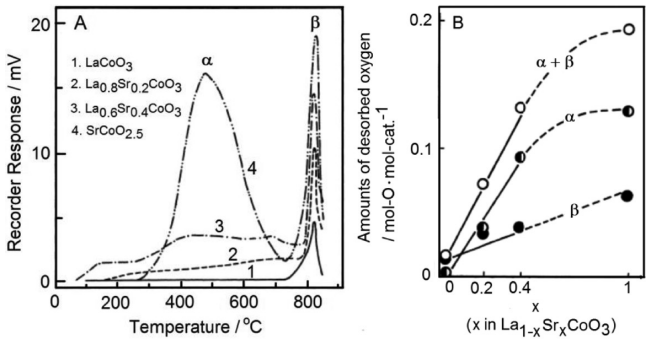

Figure 6. (A) O_2-TPD profiles of $La_{1-x}Sr_xCoO_3$, which was recorded at a heating rate of 10 °C min^{-1}; (B) Dependence of the amount of desorbed oxygen on x of $La_{1-x}Sr_xCoO_3$.[112]

°C was attributed to the desorption of ordinarily chemical adsorbed oxygen. The small peak area indicates that this oxygen is difficult to generate or the amount is small. The peak at temperature 300−700 °C was attributed to the oxygen desorbed from oxygen vacancy (denoted as α oxygen), and its amount increased with the x for $La_{1-x}Sr_xCoO_3$, indicating that the substitution of low-valence Sr^{2+} for high-valence La^{3+} leads to the increase of oxygen vacancy, which can be explained by the principle of electroneutrality. Similarly, the amount of lattice oxygen desorbed from the catalyst, which appeared at above 700 °C and was denoted as β oxygen, increased also with the increase of x for $La_{1-x}Sr_xCoO_3$, indicating that the substitution of La^{3+} by Sr^{2+} could promote the mobility of lattice oxygen or loosen the Co−O bond. Further, it was found that the sum of $\alpha + \beta$ oxygen was related to the Sr content, as shown in Figure 6B, suggesting that the oxygen absorption is associated with some sort of lattice defect originating from the partial substitution of Sr.

3.4. X-ray Photoelectron Spectroscopy. A variety of measurements that detect the surface chemistry of material have been applied in catalysis. Among them, the X-ray photoelectron spectroscopy (XPS) is a surface-sensitive technique and provides information on the surface elemental compositions and surface chemistry of a material. In the case of perovskite oxide, the information attractive for catalysis is the surface composition and the oxidation state of oxygen and the B-site metal cations. Information from oxygen species reflects the composition of each oxygen species and the amount of oxygen vacancy generated in the structure, as that of O_2-TPD, although the B-site metal cations reflects the composition of $B^{(n+1)}/B^{n+}$ couples and could be indicative of the redox ability of the material.[112−115] The XPS information obtained for surface oxygen and the B-site metals are described separately as follow.

In response to the oxygen information obtained from the O_2-TPD experiment, Seiyama et al. also measured the O 1s XPS spectra for the $La_{1-x}Sr_xCoO_3$-based perovskite oxides, Figure 7A, showing that two types of oxygen species were detected,

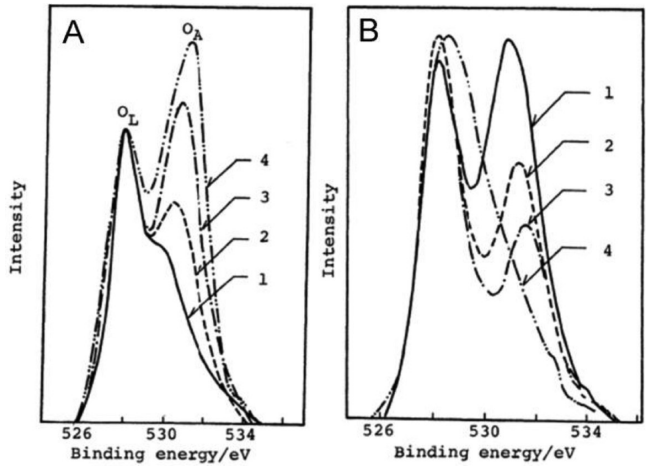

Figure 7. (A) XPS for O 1s level of $La_{1-x}Sr_xCoO_3$: (1) $LaCoO_3$, (2) $La_{0.8}Sr_{0.2}CoO_3$, (3) $La_{0.6}Sr_{0.4}CoO_3$, (2) $SrCoO_{2.5}$; (B) XPS for O 1s level of $La_{0.6}Sr_{0.4}CoO_3$: (1) R.T., (2) 300 °C, (3) 500 °C, (4) 800 °C.[112]

and the composition changed with the x value.[112] According to the XPS data booklet, it was classified that the peak situated in the range of 528−530 eV (O_L) is attributed to lattice oxygen and that in the range of 530−532 eV (O_A) is attributed to dissociative oxygen on the oxygen vacancy. Although no appreciable change in the O_L was observed, the intensity of peak O_A increased significantly with the x, indicating the increase of oxygen vacancy. This is in good agreement with the results obtained from O_2-TPD experiment.

The surface composition of the two oxygen species can be obtained by calculating the peak area of each species in the XPS spectrum, through a peak fitting method using the Gaussian function. In this analysis, the number of peaks deconvoluted and each of the peak position (which reflects the binding energy) should correspond to a definite oxygen species.

Interestingly, the authors found that the O_A signal decreased and upward shifted, and the O_L signal broadened when the sample $La_{0.6}Sr_{0.4}CoO_3$ was evacuated from R.T. to 800 °C, Figure 7B. The decrease in the intensity of O_A signal indicated that the adsorbed oxygen was desorbed gradually from the catalyst, and the upward shift suggested that the adsorbed oxygen at lower binding energy was liberated. The broadness of the O_L signal signified that a part of lattice oxygen was eliminated and that some new lattice defects and oxygen species were formed.

dx.doi.org/10.1021/cs500606g | ACS Catal. 2014, 4, 2917−2940

Table 1. Surface Element Compositions of the $La_{0.6}Sr_{0.4}Fe_{0.8}Bi_{0.2}O_3$ Samples Obtained from XPS Spectra[116]

sample[a]	Fe/La[b]	Fe/Sr[b]	Fe/Bi[b]	Fe^{4+}/Fe^{3+}[b]
LSFB−F127-H_2O	0.98 (1.33)[c]	0.83 (2.00)[c]	1.10 (4.00)[c]	0.43
LSFB-F127-EtOH	1.04 (1.33)	0.95 (2.00)	1.06 (4.00)	0.56
LSFB-PEG-EtOH	1.15 (1.33)	1.00 (2.00)	0.91 (4.00)	0.60
LSFB-Lysine-EtOH	1.22 (1.33)	1.05 (2.00)	0.97 (4.00)	0.85
LSFB-Xylitol-EtOH	1.23 (1.33)	1.13 (2.00)	0.90 (4.00)	1.24
LSFB-EG-MeOH	1.23 (1.33)	1.09 (2.00)	1.35 (4.00)	1.06
LSFB-bulk	0.90 (1.33)	0.73 (2.00)	0.70 (4.00)	0.28

[a]For meaning of the letters, see the ref 116. [b]This is the molar ratio. [c]The data in parentheses are the nominal molar ratios of the LSFB samples.

From the XPS spectrum of metal cations, information on the surface molar ratio of metals at A- and B-site, as well as the oxidation state and composition of B-site metal could be provided. As an example, Table 1 lists the molar ratio of surface metal species obtained from XPS spectra for $La_{0.6}Sr_{0.4}Fe_{0.8}Bi_{0.2}O_3$ prepared under different conditions.[116] The oxidation state of iron (e.g., Fe^{4+}/Fe^{3+}) can be confirmed by the binding energy, and their percentage can be obtained from the area of the respective peak deconvoluted using Gaussian fitting. From the surface molar ratio of Fe/La, Fe/Sr, and Fe/Bi, it can be seen that the determined value was always smaller than that of the nominal value, indicating that the La, Sr, and Bi atoms are enriched, or the Fe atoms are defected, on the surface. The enrichment of Bi atoms is especially serious as the real Fe/Bi ratio is far away from the nominal value. Considering that Fe is the major metal responsible for the catalytic performance, porous sample, which showed larger Fe/Bi ratio than the bulk, is preferable for use as a catalyst. Furthermore, it is seen that the preparation conditions significantly affects the molar ratio of Fe^{4+}/Fe^{3+}, meaning that sample with different redox properties could be obtained by adopting different preparation conditions, which offers a way to synthesize desired catalyst for special use. That is, information from XPS measurement could be used to optimize catalyst and predict its catalytic behaviors.

3.5. Temperature-Programmed Reduction of Hydrogen. Temperature-programmed reduction (TPR) is widely used for the characterization of solid materials. The technique gives quantitative information on the reducibility of the oxide's surface, as well as the heterogeneity of the reducible surface.[36,103,117−120] The procedure for H_2-TPR measurement is similar to that of O_2-TPD, except that at the final step the carrying gas is not inert (e.g., He, Ar) but a reducing gas mixture (typically 3% to 17% hydrogen diluted in argon or nitrogen). The characters of the H_2-TPR profile, including the shape, the peak area, and the temperature at the peak maximum, depend not only on the nature of the oxides but also on the hydrogen concentration and the flow rate of the reducing gas mixture, thus the profiles could be significantly different even for the same material if the measurement was done at different conditions.

For the H_2-TPR profile of perovskite oxides, it reflects mainly the redox properties of B-site metal cation, which has alterable valences. The number of reduction peaks and the sequence of them depend intimately on the nature of the B-site metal. The metal at A-site usually has stable valence (e.g., La^{3+}, Sr^{2+}) and is hard to be reduced. Thus, it can be expected that the H_2-TPR profile of perovskite, for example, $LaSrNiO_4$, should contain two reduction peaks: the first corresponds to the reduction of Ni^{3+} to Ni^{2+}, and the second corresponds to the reduction of Ni^{2+} to Ni^0, without considering the influence of La^{3+} and Sr^{2+}. The peak area reflects the number of species reduced, which can be calculated based on the H_2 consumption using CuO as standard,[121] whereas the temperature at peak maximum (T_{max}) reflects the reducibility of the species. Lower T_{max} normally corresponds to stronger reducibility, but in some cases, the total amount of H_2 consumed should be considered, which may lead to delayed T_{max} due to the large amount of H_2 consumed.

Figure 8A depicts the H_2-TPR profiles of samples $LaB_{1-x}B'_xO_3$ (B = Mn, B′ = Cu, Zn, Ni).[121] In order to classify the reduction peaks, the H_2-TPR profiles of simple oxide for each metal was also presented (Figure 8B). La_2O_3 and ZnO that have no variable oxidation state showed negligible reduction peaks, thus the reduction of La^{3+} and Zn^{2+} in the corresponding perovskite oxides can be neglected. Mn^{4+} is stable in simple oxide (MnO_2), thus the reduction of Mn occurs from Mn^{4+} to Mn^{3+} and further to Mn^{2+}. The reduction of them occurs at a temperature range of 302−331 and 400−450 °C, respectively.[121,122] The reduction of NiO occurs at 456 °C with a shoulder peak attributed to the reduction of Ni^{3+} appearing at 367 °C.[123] The reduction of Cu^{2+} to Cu^0 in CuO showed one reduction peak at a temperature of 330 °C.

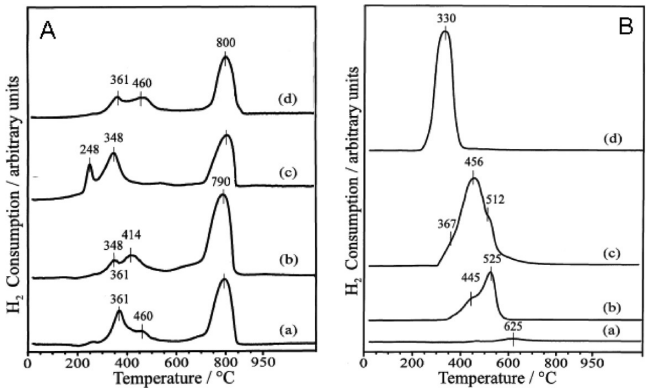

Figure 8. TPR profiles obtained from (A) perovskite oxides: (a) $LaMnO_3$, (b) $LaMn_{0.8}Ni_{0.2}O_3$, (c) $LaMn_{0.8}Cu_{0.2}O_3$, (d) $LaMn_{0.8}Zn_{0.2}O_3$; and (B) the corresponding simple oxide: (a) ZnO, (b) Mn_2O_3, (c) NiO, (d) CuO.[121]

On the basis of the above knowledge, the classification of reduction peak for each perovskite oxides can be made. For instance, the reduction peak of $LaMnO_3$ at 361 and 790 °C is attributed to the reaction of Mn^{4+} to Mn^{3+} and Mn^{3+} to Mn^{2+}, respectively; the reduction peak of $LaMn_{0.8}Ni_{0.2}O_3$ at 348, 414, and 790 °C is attributed to the reduction of Mn^{4+} to Mn^{3+}, Ni^{3+} to Ni^{2+}, and Mn^{3+} to Mn^{2+}, together with Ni^{2+} to Ni^0, respectively, whereas the downward shift in temperature and smaller peak area of Mn^{4+} to Mn^{3+} suggests that the substitution of Ni for Mn promotes the reducibility of Mn^{4+}

dx.doi.org/10.1021/cs500606g | ACS Catal. 2014, 4, 2917−2940

Table 2. Physical Properties and Catalytic Performance of $La_{2-x}Sr_xCuO_4$ (x = 0, 0.5, 1) and $LaSrMO_4$ (M = Co, Ni, Cu).[132]

catalysts	S.A. (m^2/g)[a]	av valence	λ[b]	NO conv. (%)[c]	NO conv. (%)[d]	red. potent. (V)	ox. potent. (V)	ΔE (V)[e]
La_2CuO_4	2.5	2.02	+0.01	1.0	1.9	2.49	3.35	0.86
$La_{1.5}Sr_{0.5}CuO_4$	2.4	2.24	−0.13	60.0	9.8	2.0	2.9	0.9
$LaSrCuO_4$	2.6	2.24	−0.38	96.8	34.3	1.30	3.13	1.77
$LaSrCoO_4$	2.3	2.85	−0.06	39.9	20.3		2.15	
$LaSrNiO_4$	2.7	2.68	−0.16	80.1	94.7	2.75	3.25	0.5

[a]BET surface area. [b]Nonstoichiometric oxygen. [c]NO reduction (reducing agent: CO) at 400 °C. [d]NO decomposition at 850 °C. [e]ΔE: the difference between oxidative and reductive potential.

and reduces its amount. For $LaMn_{0.8}Cu_{0.2}O_3$, it was suggested that the reduction of Cu^{2+} was unlike that in the simple oxide CuO as indicated by the size and shape of the first reduction peak. Thus, the reduction of Cu^{2+} in the perovskite oxide underwent a two-step reduction with Cu^{1+} as intermediate. This suggests that Cu^{1+} could be stabilized in the perovskite structure. Similar to that observed in $LaMn_{0.8}Ni_{0.2}O_3$, the reduction temperature for Mn species was altered due to the replacement by Cu species, indicating that the incorporation of external metal ion would influence the reducibility of the original B-site cation. The substitution of Zn for Mn ($LaMn_{0.8}Zn_{0.2}O_3$) did not alter the reducibility of Mn species, but reduced the H_2 consumption. This indicated that the incorporation of zinc did not influence the amount of Mn^{4+} species but caused a decrease in the oxidative nonstoichiometric oxygen.[121]

Overall, the above results indicated that H_2-TPR is not only a powerful tool in characterizing the redox properties of catalyst, which provides both quantitative and qualitative information for B-site cation at surface as that of XPS measurement, but also provides information on the reduction behaviors of B-site cation under different environments.

3.6. Other Technologies Used for Characterizing Perovskite Oxides. With the development of technology, many other methods have been developed and applied to characterize the textural and surface properties of perovskite oxides, including thermal analysis,[124,125] surface acid−base measurement,[126] MAS NMR,[127,128] FT-TR and UV−vis,[19,129−131] cyclic voltammetry (CV),[132,133] electron paramagnetic resonance (EPR),[129,134] oxygen isotope exchange,[119,135−137] and so forth. The measurements mentioned above are the most basic technologies used for characterizing perovskite oxides, which provide information on the surface oxygen species, surface composition of each atom and redox properties of B-site metal cations at surface resulted from the structural features, which critically influence the catalytic performances of the perovskite oxides. For readers who are interesting in other technologies, we refer them to the literature cited above and elsewhere.

4. APPLICATIONS IN CATALYSIS

4.1. Catalytic NO Decomposition. NO emitted from mobile vehicles and industrial plants are harmful to the environment, and their removal is an urgent affair of today.[38,138] The direct decomposition of NO into N_2 and O_2 has large negative Gibbs free energy and is regarded as one of the most ideal ways for NO removal.[34,35,139] From the NO molecular orbital: $(\sigma_{1s})^2(\sigma_{1s}^*)^2(\sigma_{2s})^2(\sigma_{2s}^*)^2(\sigma_{2p})^2(\pi_{2p})^4(\pi_{2p}^*)^1$, it can be inferred that when NO captures one external electron to fill in the (π_{2p}^*) orbital, forming NO^- anion, the bond order of N−O bond will be decreased from 2.5 to 2.0, facilitating the reaction.

Perovskite oxides with an oxygen defect have been long regarded as promising catalysts for NO removal. On the one hand, oxygen vacancy can provide space for NO adsorption, and on the other hand, electrons can be generated in the structure to activate NO, in the form of B^{4+}-(NO^-)-B^{3+}, as a result of the oscillation between B^{3+}-□-B^{3+} and B^{4+}-(e^-·□)-B^{3+}. Clearly the presence of oxygen vacancy and the redox ability of B-site cation are two major factors influencing NO adsorption and activation, and their important role in the reaction have been illuminated in many works.[35,108,140−147] Zhao et al. found, based on a NO-TPD experiment, that La_2NiO_4 with excess oxygen showed no adsorption capacity for NO at low temperature, and only at a temperature above 100 °C, where the surface oxygen is desorbed, could it show NO adsorption capacity; although for $LaSrNiO_4$ that possesses an oxygen vacancy, it showed good NO adsorption capacity even at room temperature, and a maximum value was observed at 200−250 °C. Consequently, $LaSrNiO_4$ showed far higher activity than La_2NiO_4 in the reaction, with NO conversion of 94% and 20%, respectively.[108]

Besides, from the nature of the reaction, it is known that NO decomposition is a self-redox reaction as no oxidizing or reducing agent is added to the reaction. This means that the catalyst should account for the oxidation and reduction process solely, and the redox properties of catalyst thus should be a crucial parameter to the reaction. Indeed, by measuring the redox potentials of two series of perovskite oxides: $La_{2-x}Sr_xCuO_4$ (x = 0, 0.5, 1) and $LaSrMO_4$ (M = Co, Ni, Cu), it was found that the match of redox potentials is the most crucial parameter and the number of oxygen vacancy (or the redox peak area) is the next one influencing the NO decomposition activity, see Table 2.[132]

The structure of active site and reaction mechanism of NO decomposition over perovskite oxides have been widely studied, yet no consistent conclusion has been drawn up to date.[34,35,140−142] Although it is generally accepted that the active site is composed of oxygen vacancy and B-site cation, the real structure is still unknown. Teraoka et al.[140] and Shin et al.[141] reported that the active site is composed of two B-site cations and two adjacent oxygen vacancies, with the two oxygen vacancies in erective status as indicated in Figure 9A. Whereas, based on theoretical calculation and the NO decomposition activity of $LaSrNi_{1-x}Al_xO_4$ (which has nonactive Al^{3+} in the B-site) and $La_{2-x}Sr_xCuO_4$ (which has different phase structures), it was found that the structure with one lattice oxygen situated between two B-site cations and two oxygen vacancies linked to the B-site cation is more favorable for the reaction, which also suggests the importance of lattice oxygen in the active site, as indicated in Figure 9B.[35]

4.2. Catalytic NO Reduction. Although NO direct decomposition is an ideal way of NO removal, its operation in practice however encounters many problems due to the

dx.doi.org/10.1021/cs500606g | ACS Catal. 2014, 4, 2917−2940

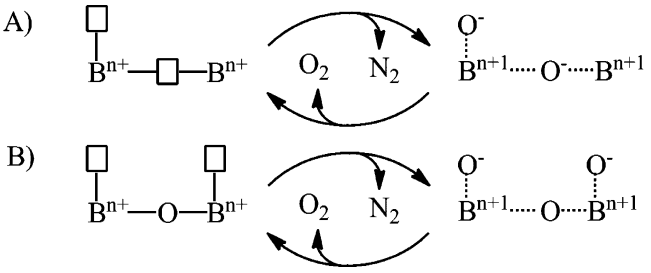

Figure 9. Proposed active site structures for NO decomposition over perovskite catalyst.[35]

kinetics limit as well as the inhibition by oxygen and poisoning by other coexisting gases such as CO_2, SO_2, and H_2O. For practical application, catalytic NO reduction is preferred, and this technology has already been industrialized. Perovskite oxides are also good catalysts for catalytic NO reduction, using either CO,[148−151] NH_3,[152−154] hydrocarbons (C_xH_y),[118,155] or H_2[156−160] as reducing agent. The presence of reducing agent compensates for the inadequacy of reducing capacity and mitigates the dependence of activity on the redox potentials of perovskite oxide catalysts. Consequently, the number of active sites might become a crucial factor influencing the activity.

As demonstrated in Table 2, when the catalysts were applied to CO + NO reduction $LaSrCuO_4$ with the largest redox peak area (which represents the number of active site or oxygen vacancy) showed the highest activity for the reaction, either for samples with different amounts of oxygen vacancy, $La_{2-x}Sr_xCuO_4$ (x = 0, 0.5, 1), or for samples with different B-site metals, $LaSrMO_4$ (M = Co, Ni, Cu). The large difference in the activity of $LaSrMO_4$ (M = Co, Ni, Cu) indicates that the type of B-site cation also is a crucial parameter influencing the activity. As can be seen from the structure of active site, for example, B^{4+}-(e^-·□)-B^{3+}, the redox property of B-site cation has a significant effect on the NO adsorption and the oxygen mobilization by generating electrons.[161] Hence, the selection of suitable B-site cation should be carefully considered when the material is prepared for use as a catalyst. The partial substitution of B-site cation with a foreign one is also effective in improving the catalytic activity, which could be partially due to a synergistic effect between them. Kaliaguine et al. reported that the substitution of Fe by Cu, and especially by Pd, in $LaFe_{1-x}(Cu, Pd)_xO_3$ can result in promoted activity for the NO + CO reaction, due to the increased amount of anion vacancies and enhanced reducibility, as well as the nature of the respective cation.[162]

The importance of redox property of B-site cation has been well documented by Hansen et al., who reported, on the basis of H_2-TPR results, that the temperature difference (ΔT) between the two reduction peaks for $M^{(n+1)+}/M^{n+}$ and $M^{n+}/M^{(n-1)+}$ of perovskite oxides, which represents the relative position of the Fermi level, has close relation to the activity of NO reduction by propene, as shown in Figure 10A.[118] The lower the ΔT is (the system is more oxidized), the higher the activity will be. This indicates that the oxidizing capacity of catalyst is more critical to the reaction than the reducing capacity, which might have been compensated by the reducing agent (propene). In contrast, it was found that big ΔT (the system is more reduced) was preferred for NO decomposition, in which no reducing agent was added, Figure 10B.[109] The different effects of ΔT on the activities suggest that the mechanism of NO decomposition and NO reduction should be different.

Significant achievements on using perovskite oxides as catalyst for NO reduction have been obtained by Nishihata et al., who found that the catalyst $LaFe_{0.57}Co_{0.38}Pd_{0.05}O_3$ can be industrialized on catalytic converters for the removal of NO using CO and C_xH_y as reducing agents.[163] They pointed out that when the catalyst was used in the oxidative and reductive atmospheres typically encountered in exhaust gas, the Pd reversibly moves into and out of the perovskite lattice. The growth of metallic Pd particles can be suppressed because of this movement, maintaining its high activity during long-term use and aging. The excellent performances of perovskite framework in accommodating and stabilizing precious metals for high-temperature use including NO removal have been observed by many authors, providing a practical route for synthesizing active and stable precious metal catalysts.[114,164−169]

Selective catalytic reduction of NO or NO_2 by NH_3 is currently the most effective technology for NOx removal from stationary combustion processes. One of the significant advantages of using NH_3 as a reducing agent is that it can reduce NOx with high selectivity even in oxygen-rich atmosphere. The commercial catalyst V_2O_5−WO_3/TiO_2 although shows satisfactory performance for the reaction; however, the problems of the toxicity of vanadia and narrow temperature window stimulate the development of new catalyst with nontoxic components, broad temperature window, as well as high catalytic efficiency for the reaction. Perovskite oxide, because of its structure feature and unique properties, was also studied on its applicability to the reaction.

In order to optimize the catalyst, Chen et al. investigated a series of perovskite oxides, with either ABO_3 or A_2BO_4 structure (A = La, B = Cu, Co, Mn, and Fe), for the reaction, finding that $LaMnO_3$ is the best catalyst, with 78% NO conversion at 250 °C.[152] Further studies indicated that the

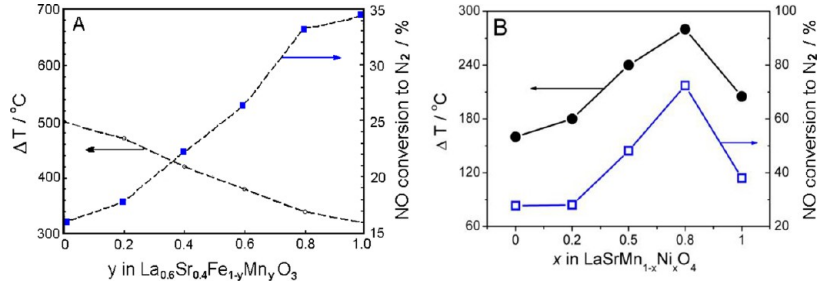

Figure 10. Relationships between the difference in temperature (ΔT) and NO removal activity: (A) Conversion of NO to N_2 from reaction "C_2H_6 + O_2 + NO" conducted on $La_{0.6}Sr_{0.4}Fe_{1-y}Mn_yO_3$;[118] (B) NO decomposition activity on $LaSrMn_{1-x}Ni_xO_4$ in the presence of 2.5 v/v% O_2 at 850 °C.[109]

dx.doi.org/10.1021/cs500606g | ACS Catal. 2014, 4, 2917−2940

coverage of inert ionic nitrates was crucial to improve NO conversion at the high-temperature zone, whereas an increase in NO oxidation ability was important at temperatures below 200 °C.[154] Mechanism investigation showed that the reaction obeyed a Langmuir−Hinshelwood mechanism, in which the NH_3 chemical adsorption was the rate-determining step, and the interaction between NH_4^+ ionic species and nitrite species accounted for the reaction at low-temperature range, Figure 11.

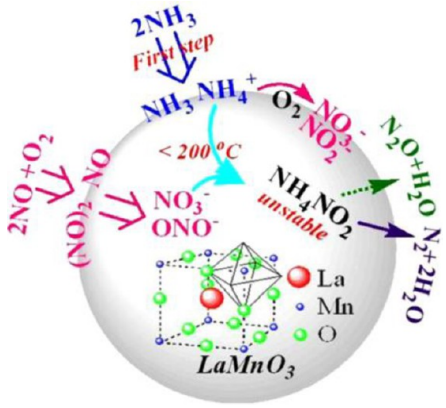

Figure 11. Proposed reaction mechanism for NH_3 SCR NO over perovskite oxides.[152]

Yang et al. investigated and compared the catalytic performances of $LaMnO_3$ and $BiMnO_3$ for NH_3 SCR (selective catalytic reduction) NO reaction at a temperature range of 100−240 °C, showing that $BiMnO_3$ was more efficient than $LaMnO_3$, especially at lower temperatures (100−180 °C), with NO conversion of 85% at 100 °C, Figure 12.[153] The high NO

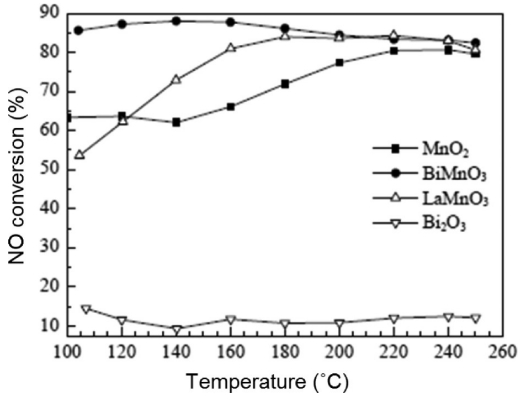

Figure 12. Catalytic activities for NH_3 SCR NO over different catalysts. Reaction conditions: 0.24 mL of catalyst, total flow rate = 40 mL/min, GHSV = 10 000 h^{-1}, 0.1% NH_3, 0.1% NO, 5% O_2, Ar balance.[153]

conversion at such low temperature indicated the potential of $BiMnO_3$ as an industrial catalyst for NH_3 SCR NO reaction. By comparison, they pointed out that the better catalytic performances of $BiMnO_3$, relative to $LaMnO_3$, for the reaction was due to the abundance of Lewis acid sites as well as the high concentration of surface oxygen.

The reduction of NO by H_2 is also a promising route for NO removal. As hydrogen, being a clean reducing agent, will not produce secondary pollution, and further, the reduction occurs at lower temperature range than that using CO, C_xH_y, and NH_3 as reducing agent. Forni et al. investigated a series of $La_{0.8}Sr_{0.2}BO_{3+\delta}$ (B = Mn, Fe, Co or Ni) catalysts and found that cobalt was the best B-site cation for the reaction, with activity order of Co > Ni > Mn > Fe.[159] The crucial factors that influenced the activity were the number of oxygen vacancy and the nature of B-site cation. It was suggested that the reduction of catalyst by H_2 to generate oxygen vacancy was an important step of the reaction mechanism.[170] Indeed, Fino et al. found that the activity of $LaFeO_3$ can be greatly increased when La^{3+} was partially replaced by Sr^{2+} (i.e., $La_{0.8}Sr_{0.2}FeO_3$) but then decreased when La^{3+} was further replaced by Ce^{4+} (i.e., $La_{0.7}Ce_{0.1}Sr_{0.2}FeO_3$). The best activity was found for $La_{0.8}Sr_{0.2}Fe_{0.9}Pd_{0.1}O_3$, in which part of Fe was replaced by Pd, with T_{50} (temperature at 50% NO conversion) of 130 °C. The authors also pointed out that the presence of oxygen affected the activity significantly (Figure 13). The activity increased with the reaction temperature and 100% N_2 yield could be achieved at 175 °C, whereas a maximum N_2 yield (ca. 73%) was observed at 125 °C in the presence of 5% O_2. The low selectivity to N_2 at higher temperature was suggested to be attributed to the formation of other nitrogen oxides species (e.g., N_2O, NO_2) as well as the consumption of H_2 by O_2.[156]

4.3. Catalytic NO Oxidation. In the SCR technology for removing NO emitted from lean-burn engine, it is believed that NO_2 is an intermediate of the reaction, using either C_xH_y or NH_3 as reducing agent.[171−177] That is, NO was oxidized to NO_2 before reacting with the reducing agent. The ability to oxidize NO into NO_2 thus could be a prerequisite in optimizing catalyst for industrial application. Traditional precious metals such as platinum are active for NO oxidation and have been widely used for diesel exhaust after-treatment.[178,179] However, they are expensive and are prone to aggregate, and thus there are still great demands for low-cost, efficient, and durable NO oxidation catalysts.[171]

The catalytic performances of perovskite oxides for NO oxidation were widely studied in recent years because of their excellent performances in NO decomposition and reduction reaction. Shen et al. investigated the catalytic performance of $LaMeO_3$ (Me = Mn, Fe, Co) perovskites prepared by the sol−gel method and found that $LaCoO_3$ with stronger reducibility was more efficient for the reaction, particularly after hydrothermal aging.[174] Further studies from the same group indicated that the nonstoichiometry of perovskite oxide ($LaMnO_3$) also influenced the NO oxidation activity. $La_{0.9}MnO_3$ with richer Mn atoms and higher Mn^{4+}/Mn^{3+} ratio showed better catalytic performances at low-temperature range due to the more easily regenerated oxygen associated with Mn^{4+}.[173] Besides the influence of B-site transition metals and nonstoichiometry, Li et al. reported that synthesis conditions were also important in preparing perovskite oxides for NO oxidation. Samples prepared with faster heating rate during the calcination process produced various impurities, decreased the surface excessive oxygen, lowered the surface oxygen, and caused particle aggregation, leading to lower activity. Consequently, the synthesis with low heating rate conditions was suggested.

Li et al. reported that perovskite oxides could also work in simulated exhaust condition with comparable activity for NO oxidation to precious metals.[171] They found that the activity of $LaCoO_3$ can be significantly improved when 10 mol % of Sr was doped for La (i.e., $La_{0.9}Sr_{0.1}CoO_3$), with NO conversion of ca. 86% at 300 °C, which is about 30% higher than the commercial DOC catalyst, Figure 14. However, the doping of

dx.doi.org/10.1021/cs500606g | ACS Catal. 2014, 4, 2917−2940

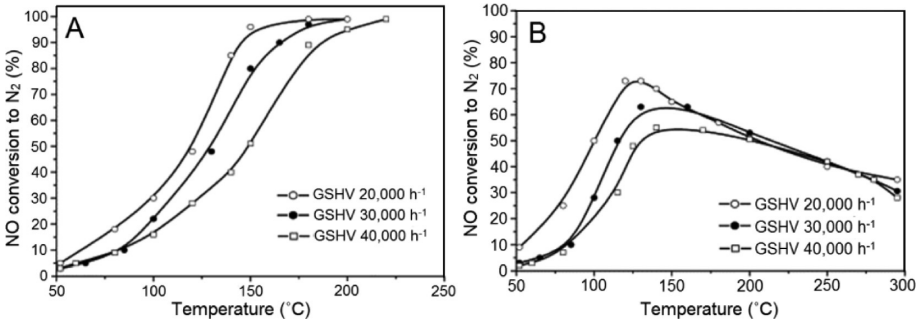

Figure 13. NO conversion to N_2 on powder $La_{0.8}Sr_{0.2}Fe_{0.9}Pd_{0.1}O_3$: (A) 1000 ppm of NO, 4000 ppm of H_2, He balance and (B) 1000 ppm of NO, 10 000 ppm of H_2, 5% O_2, He balance.[156]

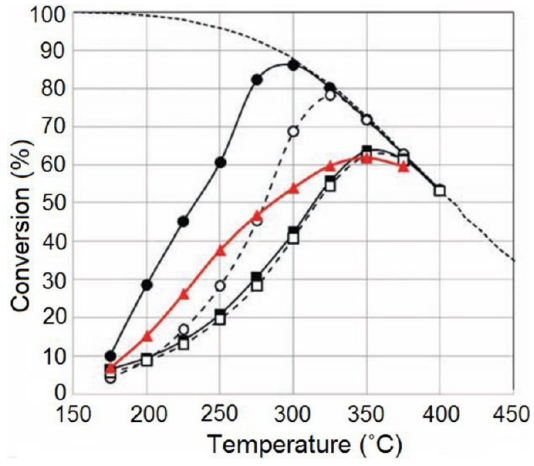

Figure 14. NO oxidation activities for $LaCoO_3$ (○), $La_{0.9}Sr_{0.1}CoO_3$ (●), $LaMnO_3$ (□), $La_{0.9}Sr_{0.1}MnO_3$ (■), and commercial DOC (▲) at a gas hourly space velocity of 30 000 h^{-1}; 400 ppm (ppm) of NO and 8% of O_2 in a balance of N_2.[171]

Sr in $La_{0.9}Sr_{0.1}MnO_3$ produced no appreciable improvement for the reaction, possibly due to the generation of oxygen vacancy by doping Sr^{2+} for La^{3+} was largely neutralized by the formation of high valence Mn^{4+}. This is different from $LaCoO_3$, in which the highest stable oxidation state for cobalt is +3.

4.4. Catalytic N_2O Decomposition. As well as NO and NO_2, N_2O is also an exhaust gas emitted from a high-temperature internal combustion engine. Although N_2O is not harmful to the human bodies, it is a rather strong greenhouse gas and is a potential contributor to the destruction of the ozone layer in the stratosphere.[180−183] Thus, catalytic N_2O removal is also essential in the application of catalyst for NO−NO_2 elimination. As demonstrated above, because of the serious problems such as high-cost, low thermal and hydrothermal stability encountered by precious metals[184−186] and zeolite,[187−190] the application of perovskite oxides for N_2O removal is of great importance.[191−200]

Screening tests on perovskite catalysts $LaBO_3$ (B = Cr, Mn, Fe, and Co) indicated that cobalt was the best transition metal for N_2O decomposition, with 50% conversion of N_2O at 455 and 490 °C in the absence and presence of 5% oxygen, respectively.[197] Similar conclusions were also obtained for Sr-doped materials as reported by Gunasekaran et al., who found that the N_2O decomposition activity decreased in the order of $La_{0.8}Sr_{0.2}CoO_{3-\delta}$ > $La_{0.8}Sr_{0.2}FeO_{3-\delta}$ > $La_{0.8}Sr_{0.2}MnO_{3-\delta}$ > $La_{0.8}Sr_{0.2}CrO_{3-\delta}$.[192] The good activity of $LaCoO_3$ can be retained even the material was deposited on a ceramic honeycomb monolith under an industrial GHSV value of 10 000−30 000 h^{-1}. The good catalytic activity of $LaCoO_3$ for N_2O decomposition, relative to that of samples with other transition metals, was found to be due to its better reducibility during the TPR runs. A recent work reported by Dujardin et al. revealed that the surface composition of catalyst also influenced greatly on the activity of N_2O decomposition. Sample with La deficiency or surface Co enrichment was favorable for the reaction at medium and high temperature, likely due to the improvement of oxygen mobility.[196]

Besides the B-site transition metal, the substitution at A-site cation has also a significant effect on the catalytic performances. Labhsetwar et al. found that the substitution of Ba^{2+} for La^{3+} or Pr^{3+} in $LaMnO_3$ or $PrMnO_3$ showed promotional effect for

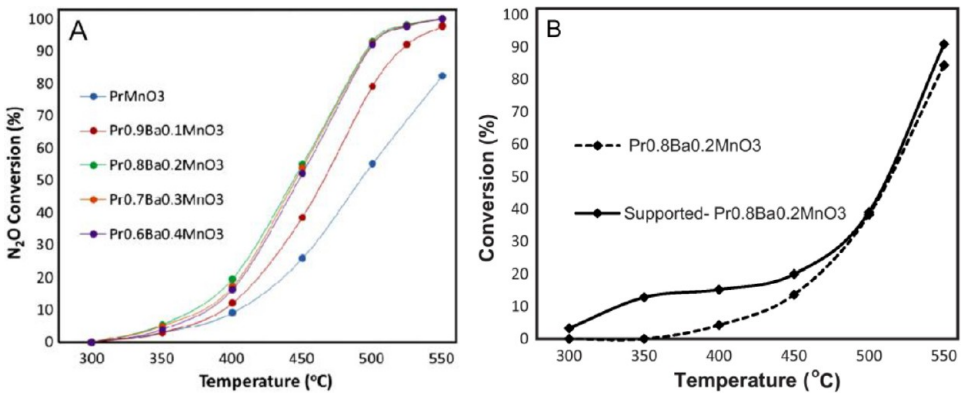

Figure 15. N_2O decomposition as a function of temperature for (A) $Pr_{1-x}Ba_xMnO_3$ (x = 0.0−0.4) and (B) $Pr_{0.8}Ba_{0.2}MnO_3$ with and without support in the presence of 200 ppm of NO and 5% O_2.[193,195]

dx.doi.org/10.1021/cs500606g | ACS Catal. 2014, 4, 2917−2940

N_2O decomposition, with the optimum value at 20% substitution (i.e., $La_{0.8}Sr_{0.2}MnO_3$ or $Pr_{0.8}Sr_{0.2}MnO_3$), Figure 15A. The promoted catalyst can be deposited on a ceramic honeycomb monolith without losing its activity, Figure 15B.[193,195] O_2-TPD and H_2-TPR results indicated that the substitution by Ba^{2+} leads to an increase of Mn^{4+}/Mn^{3+} ratio and enhanced redox property, which are responsible for the improved catalytic activity.

Perovskite oxides can also be used as support of precious catalyst for the reaction. Granger et al. prepared and compared the catalytic performances of Pt catalysts supported on γ-Al_2O_3 and $LaFeO_3$ (i.e., 4 wt % Pt/γ-Al_2O_3 and 4 wt % Pt/$LaFeO_3$) for simultaneous reduction of N_2O and NO, finding that the latter showed better resistance to thermal sintering than the former at elevated temperature in the presence of oxygen and water.[201] The Pt particles in the former grew significantly and caused a detrimental effect to N_2O conversion at high temperature, although this did not occur in the latter, as the Pt particles can be incorporated into the $LaFeO_3$ crystal lattice and be stabilized during the thermal activation process. The stabilizing effect of perovskite for precious metals at high temperature could minimize the metal loadings and improve the catalytic performance, opening a new practical interest to prepare precious metal catalysts for industrial application.

It is well-known that the oxygen−oxygen recombination ($2O^* = O_2 + 2^*$) is the rate-limiting step in N_2O decomposition, it is therefore essential to remove the surface adsorbed oxygen immediately after its formation to allow the reaction to proceed. In this respect, Wang et al. reported that surface adsorbed oxygen can be separated using a perovskite membrane, which ensures in situ removal of surface adsorbed oxygen by reducing agent such as methane, as illustrated in Figure 16A. The active site could be rapidly regenerated

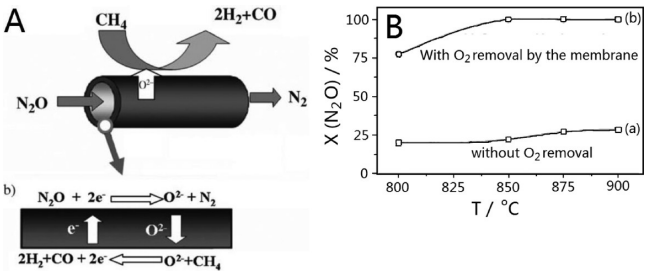

Figure 16. (A) Proposed mechanism for the direct decomposition of N_2O to N_2 with in situ removal of the rate-inhibiting surface oxygen by a perovskite hollow fiber membrane; (B) Conversion of N_2O at different temperatures with or without oxygen removal by the membrane. For experimental details, please see ref 191.

because of this in situ removal process, resulting in improved activity, as shown in Figure 16B.[191] This will also be a good strategy in applying perovskite catalysts to NOx (N_2O, NO, and NO_2) removal.

4.5. Catalytic Complete Oxidation of CO and CH_4. CO and CH_4 are also unwanted gases in the exhaust emitted from a high-temperature internal combustion engine. The removal of them over perovskite catalyst thus has practical significance especially when the catalyst is simultaneously used for NOx removal. Besides, the oxidation of CO and CH_4 are also two simple and most used model reactions, which represent two typical surface interactive processes conducted on perovskite oxides. The former is a suprafacial process, in which the catalyst surface provides a set of electronic orbitals of proper symmetry and energy for the bonding of reactant and intermediate, whereas the latter is an intrafacial process, in which the catalyst participates as a reagent that is partly consumed and regenerated in a series of continuous redox cycles.[4,202,203] Study on them thus provides evidence for the evaluation of factors that influence the surface and catalytic properties of perovskite oxides.

From the molecular formula, it is known that the oxidation of CO into CO_2 needs to capture one external atomic oxygen, without rupturing the C−O bond. Remembering that oxygen vacancy of perovskite oxides has the capability of splitting molecular oxygen into atomic oxygen and CO is a good reducing agent that can react directly with atomic oxygen, it is expected that material with more oxygen vacancy should benefit the reaction. Indeed, the dependence of CO oxidation activity on the number of oxygen vacancy has been observed in many works.[110,204−206] To generate and increase the number of oxygen vacancy is thus an interesting and attractive quest for the preparation of catalyst for CO oxidation. An obvious way is to substitute a low-valence cation for a high-valence one as demonstrated above. For instance, the substitution of Sr^{2+} for La^{3+} in $La_{2-x}Sr_xCuO_4$ could lead to a significant increase in the number of oxygen vacancy and hence increases the CO oxidation activity especially at high temperatures.[204] However, this changes the composition of material leading to confusion regarding the role of oxygen vacancy. The other way is to prepare the desired materials under different conditions while keeping the compositions unchanged. This is more desirable for investigation on the intrinsic relationship between the oxygen vacancy and the activity as influences (e.g., changes in lattice parameters) caused by substitution (i.e., metals with different oxidation states and radii) can be avoided. In this respect, Fierro et al. prepared a series of $LaCuO_{3-\delta}$ samples with different amounts of oxygen vacancy by altering the preparation conditions, and they found that the number of oxygen vacancy indeed has significant influence on the CO oxidation activity,[205] giving direct evidence for the importance of oxygen vacancy in the reaction.

Besides the number of oxygen vacancy, the redox properties of B-site cation also have significant influence on the activity. Porta et al. investigated the catalytic performances of $LaAl_{1-x}Fe_xO_3$ for CO oxidation and found that all the Fe-containing samples were substantially more active than $LaAlO_3$, thus pointing to the essential role of the redox properties of transition metal ion in developing highly active catalysts. Furthermore, based on the trends in the specific reaction rate and iron content (Figure 17A), the authors found that there existed a dilution effect and concluded that isolated iron ions are more active than iron species surrounded by oxygen bound to other iron ions. That is, the active sites contain isolated Fe ions bonded to more easily removable oxygen.[207] Optimization of B-site transition metals, based on the series $LaCo_{0.5}M_{0.5}O_3$ (M = Mn, Cr, Fe, Ni, Cu), suggested that the composition $LaCo_{0.5}Mn_{0.5}O_3$ is the most favorable.[208]

Scott et al. studied the effect of incorporating precious metal Pd at the B-site on the CO oxidation activity, finding that although the materials ($BaCe_{1-x}Pd_xO_{3-\delta}$) have low surface area (1.0 m^2 g^{-1}), they showed comparable activity to highly dispersed PdO/Al_2O_3 catalyst due to the incorporation of Pd. This suggests that active Pd catalyst can be obtained by inserting it into a perovskite framework. The presence of cationic Pd(II) in the framework is essential, as the activity

dx.doi.org/10.1021/cs500606g | ACS Catal. 2014, 4, 2917−2940

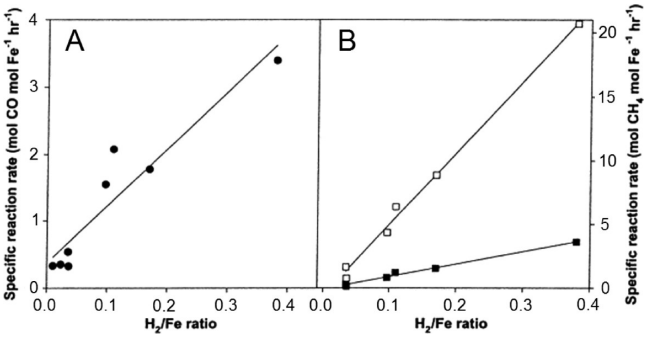

Figure 17. Reaction rate referred to catalyst weight as a function of H_2/Fe ratio: (A) CO oxidation at 300 °C; (B) CH_4 combustion at 500 °C (filled square) and at 600 °C (open square).[207]

declined dramatically when it was extruded out in Pd(0) form. However, the extruded Pd(0) can re-enter the framework if the sample was reoxidized and its activity could be recovered, as shown in Figure 18.[209]

In addition to the natural of catalyst such as oxygen vacancy and redox properties of B-site cation, the surface crystallinity was also reported to be important for the reaction. Taguchi et al. found that $LaCoO_3$ prepared using ethylene glycol and citric acid, although possessing low surface area, showed better activity to that prepared using ethylene glycol only, as a result of its better surface crystallinity.[210]

Investigation on the reaction by oxygen isotopic exchange technology indicated that the atomic oxygen which had reacted with the CO was not derived exclusively from molecular oxygen in the reacting gas. That is, the lattice oxygen in the perovskite framework can react with the adsorbed CO to generate an oxygen vacancy, whereas the molecular oxygen can be dissociated into atomic oxygen on the oxygen vacancy and fill the framework as lattice oxygen,[135,211] as illustrated in Figure 5B. Hence, the mobility of lattice oxygen, or the bond strength of B−O bond, is also a criterion to evaluate the catalytic performances of perovskite oxides.

Relative to CO oxidation, the dependence of CH_4 oxidation on the oxygen vacancy is weak, as it belongs to different types of reactions (suprafacial vs intrafacial). This can be verified from the catalytic performances of $LaSrCuO_4$ and $LaSrNiO_4$. The former with more oxygen vacancy showed better activity to CO oxidation, whereas the latter with more matched redox potentials is more favorable for CH_4 oxidation (Figure 19A).[203] That is, the redox properties of B-site cation are more crucial to CH_4 oxidation, implying a different reaction mechanism relative to CO oxidation. The oxygen vacancy should benefit the reaction as it is involved in the active site, which can be confirmed by the increased CH_4 oxidation activity from La_2CuO_4 to $La_{1.5}Sr_{0.5}CuO_4$ and further to $LaSrCuO_4$.[203] In understanding the nature of CH_4 oxidation conducted over perovskite oxides, Marchetti and Forni studied the reaction carefully over $LaMnO_3$-based catalysts.[212] Using oxygen isotope technology, they found that although sample with more oxygen vacancies was more active for the suprafacial oxygen exchange reaction (e.g., $^{18}O_{2(g)} + 2^{16}O_{(s)} = 2^{18}O_{(s)} + {}^{16}O_{2(g)}$), it showed the least activity for CH_4 combustion. On the basis of experimental results, they concluded that the activity depended mainly on the temperature of oxygen desorption peak maximum (T_{max}), which is an index of the mobility of lattice oxygen, Figure 19B. That is, the lattice oxygen of catalyst participates in the reaction as a reactant, indicative of an intrafacial reaction. In order to utilize the energy released from CH_4 oxidation, it has been suggested to conduct the reaction in a microscale combustion reactor, which is an energy resource developed in recent years for portable power production.[213]

As for the active site, Porta et al. investigated the CH_4 oxidation reaction over $LaAl_{1-x}Fe_xO_3$ and found that the specific reaction rate decreased with the Fe content (Figure 17B), thus proposing that the active site composed of isolated B-site ions bonded to more easily removable oxygen.[207] Taguchi et al. found, based on the catalytic performances of $La_{1-x}M_xCoO_3$ (M = Ca, Sr, and Ba), that both the x value and the radius of M can influence the activity by altering the structure of the active site. The increase of x increased the oxidation state of Co ($Co^{3+} \rightarrow Co^{4+}$) and the increase of M radius enlarged the Co−O−Co angle, both of which facilitated the reaction.[214] A model of active site is presented in Figure 20, showing that the repulsion of adsorbed oxygen or that the amount of adsorbed oxygen depends both on the properties of Co cation and the distance between the two Co cations. High oxidation state and large distance between the two Co cations lead to decreased repulsion of the adsorbed oxygen or increased amount of adsorbed oxygen, thus improving the activity. The

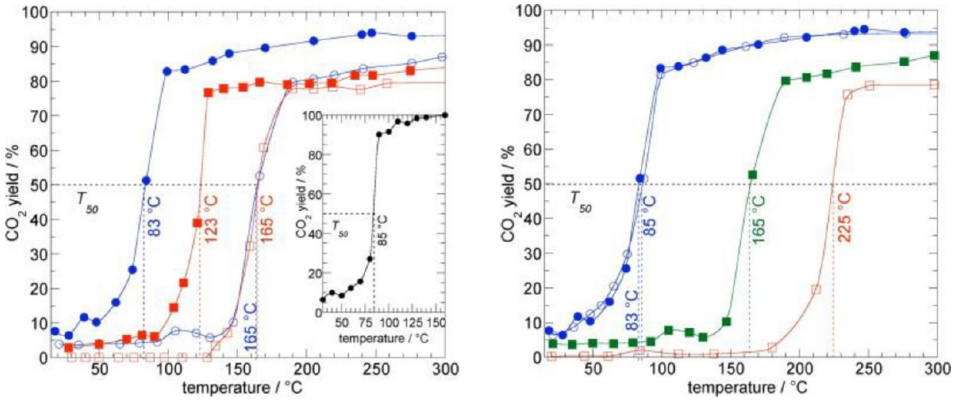

Figure 18. Temperature-programmed reaction profiles for the oxidation of CO (1000 ppm) by excess O_2 (10% in N_2, total flow rate 50 cm^3 min^{-1}) over 100 mg $BaCe_{0.90}Pd_{0.10}O_{3-\delta}$: as-prepared (solid blue circles), reduced (solid green squares), and reoxidized forms (open blue circles), as well as $BaCeO_3$ (open red squares). Lines are drawn only to guide the eye. The inset shows the profile for 45 mg PdO/Al_2O_3 (2.0 wt % Pd, black) measured under the same conditions.[209]

dx.doi.org/10.1021/cs500606g | ACS Catal. 2014, 4, 2917−2940

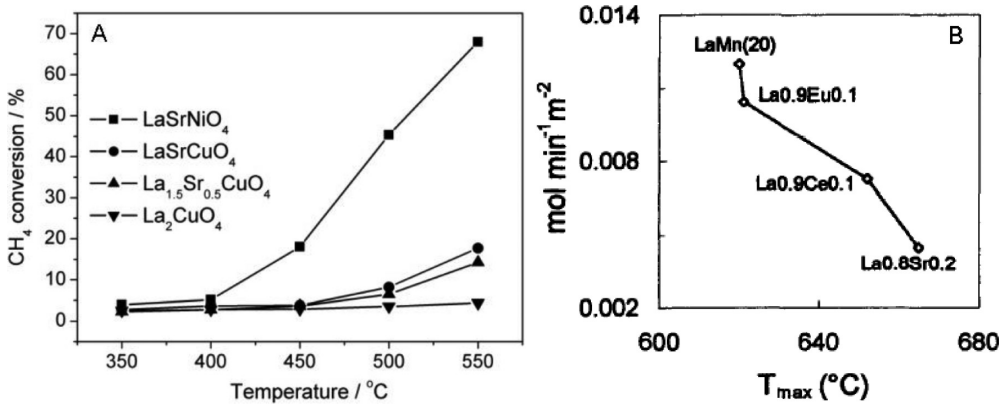

Figure 19. (A) Dependence of CH_4 conversion on reaction temperature over $La_{2-x}Sr_xMO_4$ (x = 0.0, 0.5, 1.0; M = Cu, Ni);[203] (B) Dependence of CH_4 specific activity on the temperature of oxygen desorption peak maximum (T_{max}) over $La_{1-x}A_xMnO_3$ (A = Sr, Eu and Ce).[212]

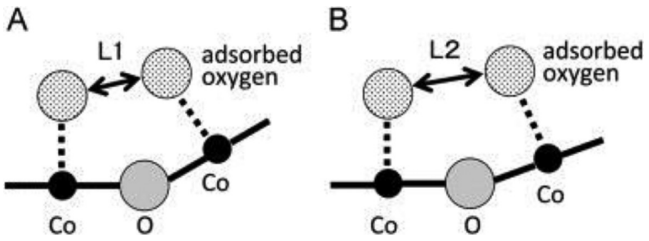

Figure 20. Model of the $(La_{0.94}M_{0.06})CoO_3$ (M = Ca, Sr, and Ba) surface: (A) a small Co−O−Co angle and (B) a large Co−O−Co angle.[214]

stability of B-site cation has also suggested to be an important factor influencing the activity.[111]

As an overall conclusion, the reaction mechanism for CO and CH_4 oxidations conducted on perovskite oxides are different. For CO oxidation, the CO molecule react directly with adsorbed oxygen ($O_{(s)}$) to give CO_2 without the participation of catalyst and the activity depends largely on the number of oxygen vacancy (Scheme 2, upper section); however for CH_4 oxidation the C−H bond was ruptured before reacting with the adsorbed oxygen, which required the catalyst to participate in as a reagent that was partly consumed and regenerated in a series of continuous redox cycles (Scheme 2, bottom section).

Scheme 2. Proposed Mechanisms for CO and CH_4 Oxidation over Perovskite Oxides[135,203]

CO oxidation:

$$O_{2\,(g)} \rightarrow 2O_{(s)} \quad (1)$$

$$CO_{(g)} \rightarrow CO_{(s)} \quad (2)$$

$$CO_{(g)} + O_{(s)} \rightarrow CO_{2\,(g)} \quad (3)$$

$$CO_{(s)} + O_{(s)} \rightarrow CO_{2\,(s)} \rightarrow CO_{2\,(g)} \quad (4)$$

CH_4 oxidation:

$$[M^{(n-1)+}O_x] + O_2 \rightarrow [O][M^{n+}O_m] \quad (5)$$

$$H_3C\text{-}H + [O][M^{n+}O_m] \rightarrow CH_3\cdot + [OH][M^{n+}O_m] \quad (6)$$

$$CH_3\cdot + [OH][M^{n+}O_m] \rightarrow [M^{(n-1)+}O_{m-3}CO_2] + 2[OH_2] \quad (7)$$

$$[M^{(n-1)+}O_{m-3}CO_2] \rightarrow [M^{(n-1)+}O_x] + CO_2 \quad (8)$$

4.6. Catalytic Oxidative Reforming of Hydrocarbon.

The current energy crisis stimulates exploration of new energy technologies to produce high-energy fuels. Hydrogen as a green and high-energy fuel receives special interest in the last decades. However, the large-scale storage and transport of pure hydrogen is a big problem because of its low density, low melting point, and the danger of explosion with oxygen, which limit its use in stationary and mobile fuel cells. In situ hydrogen generation by reforming of hydrocarbons from fossil fuels provides a way to overcome these problems and has been widely investigated.[215−218] Among the strategies, the partial oxidation of hydrocarbons using air as oxidant is more desirable, as it produces not only hydrogen, but also carbon monoxide, which is another energy resource; meanwhile, the low-cost of air makes it feasible for industrial application.

Methane is a good hydrocarbon for producing hydrogen because of the high hydrogen percentage. Besides as a catalyst for catalytic complete oxidation of CH_4, perovskite oxides also have been reported to be a good catalyst in catalyzing partial oxidation CH_4 into syngas ($CO + H_2$).[219−225] However, it should be noted that in such applications, the perovskite is not used as a real catalyst but as a precursor of catalyst. The reason for using perovskite oxide in the reaction is that it can generate catalysts with finely segregated active metals onto a matrix of metal oxides generated from the perovskite precursor after reduction.[219] Because of this, the in situ yielded catalyst showed good activity and stability for the reaction. For instance, Morales et al. reported that the use of $La_{0.5}Sr_{0.5}CoO_{3-\delta}$ perovskite as catalyst precursor led to >95% CH_4 conversion and >85% CO and H_2 selectivity at temperature above 900 °C. The catalyst showed highly stable activity to the reaction and the activity increased with the redox cycles, Figure 21.[220] Whereas, Specchia et al. found that nickel−lanthanum-based perovskite catalyst showed low catalytic activity toward the reaction, due to the high reducibility of their structures into La_2O_3, metallic Ni and Ni oxides during the reaction.[221]

On the other hand, Jiang et al. reported that perovskite oxides can oxidize CH_4 directly into CO and H_2 using its lattice oxygen as oxygen resource (in the feed gas, only CH_4 was present).[222] As a result, they found that the doping of Sr and Ca for $LaCrO_3$ or $LaFeO_3$ to increase the mobility of lattice oxygen led to enhanced CH_4 conversion. It should be noted that the perovskite oxide was not a real catalyst, which must be reoxidized (treated in O_2) when the activity was lost.

dx.doi.org/10.1021/cs500606g | ACS Catal. 2014, 4, 2917−2940

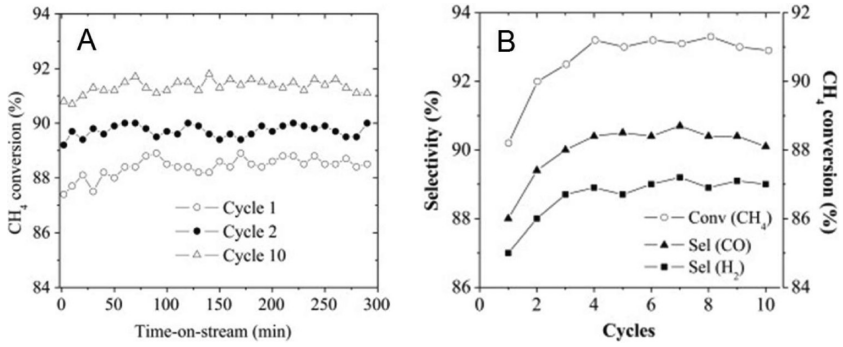

Figure 21. (A) Influence of time-on-stream on CH_4 conversion and (B) effect of redox cycles on the CH_4 conversion and selectivity to CO and H_2 over 50 mg $La_{0.5}Sr_{0.5}CoO_{3-\delta}$ at 900 °C, $CH_4/O_2/N_2$ ratio of 1.8/1/4 and 3.0×10^4 cm^3 g^{-1} h^{-1}.[220]

Besides methane, methanol, natural gas, gasoline, diesel fuel, aviation jet fuel, and ethanol could also be used as precursors to produce hydrogen, which has been well compared and summarized in a previous work.[218] In the case of hydrogen production from diesel fuel over perovskite oxide, Villoria et al. compared the effect of preparation method for the perovskite precursor $LaCoO_3$ on the catalytic performance of the resulting catalyst Co/La_2O_3, finding that catalyst resulted from $LaCoO_3$ prepared by solution combustion synthesis (SCS) showed the best long-time activity than that from samples prepared by sol–gel (PEC) and coprecipitation (COP) methods.[226] This was explained that the $LaCoO_3$ prepared from SCS has a porous network and higher homogeneity in bulk and surface than that prepared from PEC and COP methods. That is, the porosity and homogeneity of perovskite oxide is crucial in improving the activity and the catalyst's life even it is used as precursor of catalyst. Further studies pointed out that Co^0 is the active site for the reaction and the presence of $La_2O_2CO_3$ phase could inhibit coke deposition on the surface.

4.7. Catalytic Combustion of Volatile Organic Compounds (VOCs). Volatile organic compounds (VOCs) emitted from many industrial processes and transportation activities, such as power generation, vehicle emissions, and solvents employment, are harmful and dangerous both to environment and human beings.[227−229] The removal of these emitted VOCs, as well as NOx, CO, and CH_4 mentioned above, is a crucial topic in the field of environmental protection. The conventional approach of disposing highly concentrated VOC streams is thermal incineration, which, however, needs to be operated at high temperature range (800−1200 °C) and requires high operating costs. Furthermore, undesirable byproducts such as dioxins and nitrogen oxides could be produced during the incineration process. In contrast, catalytic combustion is an effective and feasible technology for VOC removal, which can be operated at dilute VOCs effluent streams (<1%) and low-temperature ranges (<600 °C) and thus has been widely investigated in the recent years. Current efforts on this technology concentrate mainly on developing efficient and low-cost catalysts, which can catalyze the complete oxidation of VOCs into CO_2 at low temperature.

Use perovskite oxides as catalysts for catalytic combustion of VOCs have attracted great attention over the years because of its low-cost, stable structure, and especially, excellent catalytic performances and great achievements have been obtained.[230−238] It has been shown that the oxidation rate depends on the bond dissociation energy of the weakest C−H bond of the VOCs,[231,239,240] which can be achieved, from another point of view, by altering the oxidation state of B-site cation, the redox properties of different B-site cation, and the surface oxygen deficiency.

In the case of the effect of B-site cation, Porta et al. studied the catalytic performances of $LaMnO_3$ and $LaCoO_3$ for VOCs combustion and found that the former that contains multivalence (Mn^{4+} and Mn^{3+}) and more surface oxygen species showed better activity than the latter that contains exclusively Co^{3+}, pointing out the importance of the redox properties of the B-site cation.[234] Pecchi et al. later investigated the effect of Ni substitution on the catalytic performances of $LaFe_{1-y}Ni_yO_3$ for VOCs combustion, finding that the intrinsic activity (mol m^{-2} h^{-1}) increased substantially with the Ni substitution, but decreased at full Ni substitution (Table 3).[233] After analysis on the phase structure and the change in the catalytic activities, they found that segregation of NiO phase took place when Fe was partially substituted by Ni, and thus concluded that the increased activity of $LaFe_{1-y}Ni_yO_3$ is attributed to a cooperative effect of between $LaFe_{1-y}Ni_yO_3$ and NiO phases, the later has stronger capability to oxygen activation.

Table 3. Ignition Temperature (T_{50}) and Intrinsic Activity at Conversion Level below 10% of Ethanol and Acetyl Acetate on $LaFe_{1-y}Ni_yO_3$ Perovskites.[233]

	y	T_{ign}^{50} (°C)		intrinsic activity	
		ethanol	acetyl acetate	ethanol (200 °C)	acetyl acetate (250 °C)
$LaFeO_3$	0.0	247	340	0.012	0.010
$LaFe_{0.9}Ni_{0.1}O_3$	0.1	222	325	0.033	0.075
$LaFe_{0.8}Ni_{0.2}O_3$	0.2	218	293	0.12	0.12
$LaFe_{0.7}Ni_{0.3}O_3$	0.3	220	282	0.22	0.23
$LaNiO_3$	1.0	250	300	0.13	0.19

Besides the intrinsic influence of the B-site cation, the preparation method was also found to be an important factor influencing the catalytic performances. Guo et al. prepared a series of $LaMnO_3$ samples by citrate sol–gel (SG), glycine combustion (GC), and coprecipitation (CP) methods and investigated their activities for toluene combustion, finding that the sample prepared by the SG method, which exhibited higher surface area, stronger low-temperature reducibility and more surface adsorbed oxygen species, showed better activity than that prepared by GC and CP methods. Dai et al. found that $LaMnO_3$ fabricated with three-dimensionally ordered macroporous (3-DOM) structure exhibited faster reaction rate for toluene combustion than the bulk one, and showed stable activity for at least ca. 50 h (see Figure 22) because of the

dx.doi.org/10.1021/cs500606g | ACS Catal. 2014, 4, 2917−2940

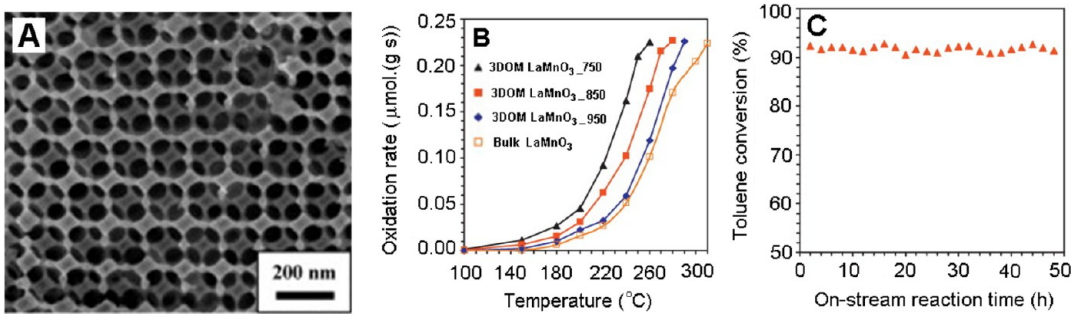

Figure 22. (A) TEM image for 3-DOM $LaMnO_3$ prepared at 750 °C; (B) Comparison in the reaction rates of toluene oxidation over 3-DOM $LaMnO_3$ prepared at 750, 850, and 950 °C and that of the bulk sample; (C) Long-term stability of 3-DOM $LaMnO_3$_750 for toluene oxidation.[241]

improved surface area, surface oxygen species, low-temperature reducibility, as well as the bimodal pore structure.[241] Whereas high temperature calcination (e.g., 750, 850, and 950 °C) would lead to collapse of pores and low surface area for the 3-DOM $LaMnO_3$, and as a consequence, low reaction rate. These results suggested that external conditions, as well as the intrinsic factors (e.g., the type of B-site cation, the number of surface oxygen defect), are also crucial in optimizing the catalytic performances.

In addition to the nature of catalyst, Monceaux et al. found that the reactant atmospheres (mixture) also can affect the oxidation behavior, and a "mixture effect" was observed depending on the composition of the mixture.[230] Generally, the component that can be preferentially adsorbed is oxidized as normal, but for other components, the temperature for complete oxidation will be raised due to the competition and interference between the reactants. Exceptionally, it was found that the temperature for complete oxidation of both acetone and toluene was lowered in an acetone−toluene mixture, indicating a positive mixture effect. The reaction mechanism however is still unknown, and it seems that no law could be applied to predict the behavior of each component.

4.8. Soot Oxidation. Diesel soot is another type of pollutant emitted from engines which needs to be removed from the atmosphere for environmental purification.[120,242−253] Unlike NOx, CO and CH_4, soot is solid which cannot diffuse and spread freely on the catalyst's surface. Hence, catalytic soot oxidation is a more complex reaction and requires multifunctional catalyst. Thus, the contact efficiency between the soot and the catalyst should be crucial for catalytic activity.

In earlier works, Kagawa et al. found that perovskite oxides showed improved activity relative to the transition metal simple oxides, and the substitution of potassium at A-sites, in particular at atomic percentage of 10%, promoted the catalytic performances prominently (Figure 23A),[242] and the ignition temperature of soot oxidation was closely related to the reaction atmosphere.[243] The promotion effect of potassium on the catalytic performances of perovskite catalyst for soot oxidation has been observed later by many authors.[244,247] It has also been found that the ignition temperature for soot oxidation conducted in NO + O_2 atmospheres, which has the trend to form NO_2, was lower than that conducted either in NO or in O_2 atmosphere (Figure 23B) showing that the atmosphere has great influences on the reaction.

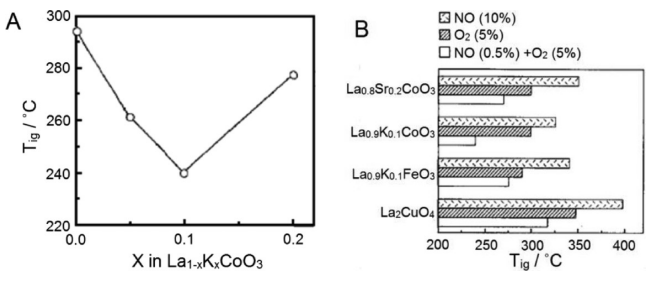

Figure 23. Effect of (A) the substitution of K for La and (B) the reaction atmosphere on the ignition temperature of soot (T_{ig})[242,243]

Fino et al. investigated and compared a series of $LaBO_3$ (B = Cr, Mn, Fe, and Ni) perovskite catalysts, with and without gold loading (2 wt %), for simultaneous oxidation of soot and CO. They found that the sample $LaNiO_3$ that possesses large amount of weakly chemisorbed O^- species exhibited the highest activity toward carbon oxidation (Table 4), indicating the key role of chemisorbed O^- species in the reaction. Although no improvement in carbon oxidation was observed, the loading of 2 wt % Au on $LaNiO_3$ decreased the T_{50} and T_{100} temperature by about 100 °C for CO oxidation because of its better capability to provide increased amount of oxygen to CO molecules relative to the pure perovskite catalyst, demonstrating that the presence of Au is essential in simultaneous removal of carbon and CO. In particular, when the 2 wt % Au-$LaNiO_3$ catalyst was lined over a SiC wall-flow monolith trap, it showed a more complete regeneration process, with 3-fold shorter time and lower amount of emitted CO, than the noncatalytic trap, which is even better than the commercial Pt/Al_2O_3 trap.[249]

Other than the physicochemical properties, Zhao et al. found that the morphology of catalyst also affected significantly the catalytic activity of soot oxidation.[245] That is, nanometric perovskite catalysts with higher ratio of surface to bulk atoms and larger surface area showed better catalytic performances for soot oxidation than the bulk because of increased contact efficiency between the catalyst and the reactants (soot and oxygen). This promoted them to synthesize a series of 3-DOM $LaCo_xFe_{1-x}O_3$ materials with high surface area for investigation in their subsequent work.[7] Indeed, the 3-DOM samples significantly decreased the ignition temperature for soot oxidation and improved the overall catalytic performances (Figure 24A). The ignition temperature could be further lowered by ca. 50 °C when the material was physically grinded to 5−20 μm, pointing out again the importance of contact area between catalyst and soot in improving the soot oxidation activity. In addition, the authors found that fine Au nanoparticles (NPs) with particle size of ca. 3 nm could be prepared and deposited on a 3-DOM $LaFeO_3$ perovskite, as shown in Figure 24B,C, thus leading to a further decreased ignition temperature (228 °C) for soot oxidation, which is due to a

dx.doi.org/10.1021/cs500606g | ACS Catal. 2014, 4, 2917−2940

Table 4. BET Specific Surface Area and Catalytic Activity Towards Both Carbon and Carbon Monoxide Oxidation of the Investigated Catalysts.[249]

catalyst	BET (m^2/g)	carbon oxidation, T_p (°C)	CO oxidation	
			T_{50} (°C)	T_{100} (°C)
Noncatalytic combustion		650	530	>750
$LaMnO_3$	16.4	524	254	315
2 wt % Au-$LaMnO_3$	17.7	525	234	290
$LaCrO_3$	15.8	506	450	580
2 wt % Au-$LaCrO_3$	22.2	505	285	500
$LaFeO_3$	29.4	524	290	340
2 wt % Au-$LaFeO_3$	18.7	525	215	240
$LaNiO_3$	14.5	430	242	280
2 wt % Au-$LaNiO_3$	10.4	431	156	197

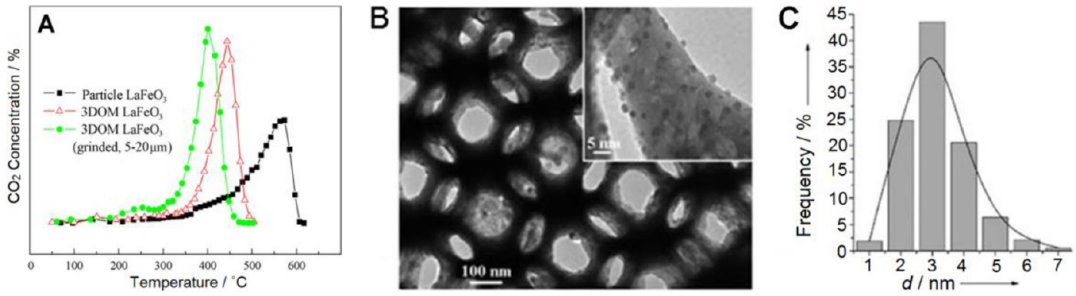

Figure 24. (A) Activity of soot oxidation conducted over the series $LaFeO_3$ samples in the presence of 5% O_2 and 0.2% NO;[7] (B) TEM image and (C) size distribution of Au NPs of 3-DOM $Au_{0.04}/LaFeO_3$.[246]

synergistic effect between the Au NPs and the perovskite oxides.[246]

Poisoning test on the perovskite oxides is essential before its possible industrialization as the component of real exhaust is rather complex, containing various pollutants that would poison or deactivate the catalysts. Many efforts on this aspect have been attempted over the years because of the industrial interest.[254−258] Among them, the poisoning by SO_2 receives special attention because residual sulfur in the fuels is inevitable and perovskite oxide is sensitive to SO_2 because of its basic properties, resulting in the formation of sulfate, which would block the accessibility of reactant to the perovskite surface and change the surface properties. Although, according to current knowledge, the poisoning by SO_2 is still not well-resolved, some achievements indicated that the incorporation of Ce,[259−261] in particular noble metals (e.g., Pt,[255] Pd[262,263]), could alleviate or slow the poisoning process, directing a way to prepare the perovskite oxide catalyst for industrial application.

Besides SO_2, the effect of other pollutants on the catalytic performances of perovskite has also been widely studied. Zhang et al. made a comprehensive study on the effect of various gases such as O_2, hydrocarbons, CO, H_2, NOx and water vapor on soot combustion over $LaCoO_3$ perovskite, finding that the presence of these gases would promote the combustion rate.[254] The presence of O_2 could promote the reaction by supplying oxygen atoms to form CO_2. Even when 1% O_2 was presented, the reaction rate could be significantly improved. High oxygen concentration could further promote the reaction rate, but the degree is less. The presence of CO could affect the catalyst from two ways: one is to react with metals to form carbonates, which are harmful to oxidation reactions, and the other is to react with oxygen to generate oxygen vacancy, which is favorable for oxidation reactions. The former occurs rarely, and the latter has a strong trend in most cases, thus leading to promotion in the activity. The presence of H_2O also has the ability to promote the reaction rate of soot oxidation, by a water−gas reaction $C + H_2O = CO + H_2$ and/or by a water−gas-shift (WGS) reaction $CO + H_2O = CO_2 + H_2$. As a consequence, the presence of hydrocarbons, for example C_3H_6, can significantly improve the reaction rate, as it on the one hand can react with the oxygen of catalyst to generate oxygen vacancy, and on the other hand, it can yield H_2O to promote the soot oxidation process. However, the presence of CH_4 has little contribution to the reaction as its combustion requires high temperature. Similar as O_2, the presence of NOx can promote the soot combustion rate by supplying oxygen atoms. It is noticed that NO_2 is more favorable for the reaction relative to NO, which could be that the former has stronger oxidizing ability than the latter.

4.9. Oxidation Removal of Organic Dyes in Aqueous Solution. It is generally believed that oxygen vacancy is an important feature of perovskite oxides and plays an important role in oxidation reactions conducted at high temperatures, because it is involved in the active site. However, the situation may be different when the material is applied to low-temperature oxidation reactions, especially for those involving unstable reactants such as H_2O_2, which will be catalytically decomposed at strong oxidizing environment. Consequently, the reactants will be consumed before participating in the reaction, leading to decreased activity, although the reaction itself needs the oxidizing ability of the catalyst. In such cases the number of oxygen vacancy and the redox properties of B-site cation in the catalyst should reach a compromised state in order to guarantee the proceeding of the reaction.

One case of such reactions is the use of perovskite as a "Fenton-like" catalyst for the oxidative degradation of organic dyes in aqueous solution. Their high hydrothermal stability guarantees well their applications in aqueous medium even in

dx.doi.org/10.1021/cs500606g | ACS Catal. 2014, 4, 2917−2940

wide pH ranges without affecting the structural stability. Comparing with the classic Fenton catalysts (dissolved Fe(II) and H_2O_2, pH < 4),[264,265] perovskite oxide is in solid phase and can thus be easily separated from the aqueous solution and used repeatedly, as expected for industrial applications.

Perovskite oxides are promising catalysts for oxidative degradation of organic dyes using H_2O_2 as oxidant.[41,266−269] Tang et al. reported that $BiFeO_3$ perovskite is a highly active and stable catalyst for oxidation removal of organic pollutants using H_2O_2 as oxidant, with an apparent rate constant 20-fold higher than that of Fe_3O_4 MNPs for Rhodamine B (RhB) oxidation and TOC (total organic carbon) removal reaching ca. 90%.[266] Nie et al. found that the substitution of Cu for Ti in $LaTi_{1-x}Cu_xO_3$ can significantly improve the activity for RhB oxidation using H_2O_2 as oxidant.[267] By substitution with copper, the La/Ti system was converted from $La_2Ti_2O_7$ to $LaTiO_3$, resulting in the production of Ti^{3+} from Ti^{4+} in the perovskite structure, which could show high Fenton catalytic activity. Simultaneously, part of Cu^{2+} could be reduced to Cu^+ in the perovskite structure. The coexistence of redox couples (Ti^{3+}/Ti^{4+} and Cu^+/Cu^{2+}) facilitated the conversion of H_2O_2 into active radical OH· (Figure 25), which was the intermediate

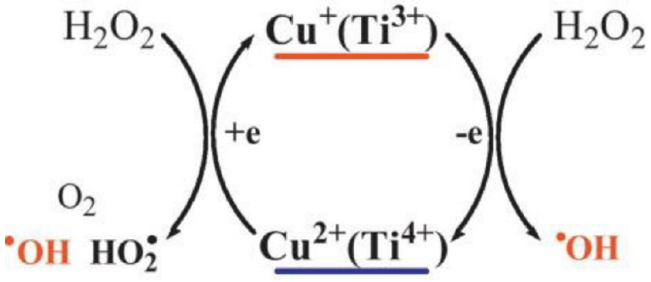

Figure 25. Proposed reaction route for H_2O_2 conversion into OH· radical over $LaTi_{1-x}Cu_xO_3$.[267]

reacting with organic dyes, thus improved degradation activity could be obtained. However, catalyst with strong oxidizing ability and/or more amounts of oxygen vacancy would destroy the reaction by catalyzing H_2O_2 decomposition.[41]

The above-reported catalysts were, however, mainly in the bulk phase with low surface area (ca. 8.5 m^2/g) and low atomic utilization, which may limit their industrial application. In order to overcome this limit, it is suggested to prepare the catalyst in nanosized structure by depositing it onto a high-surface-area support. Sample with small particle size on one hand can alter the surface properties due to a quantum effect, and on the other hand, it can improve the contact area with the substrates, guaranteeing the sufficient supply of substrate to the reaction and improving the atomic utilization. Besides, considering that the reaction is normally conducted at atmospheric environment at which conditions the oxidation reaction belongs to a suprafacial process, thus the increase in surface area would lead to the exposure of more active site, which is the main factor influencing the catalytic efficiency, as demonstrated before.

SBA-15 supported $LaFeO_3$ (i.e., $LaFeO_3$/SBA-15) was synthesized and used to RhB oxidation. XRD patterns and TEM image indicated that $LaFeO_3$ with perovskite structure can be well formed and dispersed over SBA-15 (cf. Figure 2), with particle size of 10−20 nm while retaining the porous structure of SBA-15 fully intact.[41] As expected, $LaFeO_3$/SBA-15 showed better catalytic activity to RhB oxidation than the bulk $LaFeO_3$, Figure 26A, despite that the real amount of $LaFeO_3$ in the former (weight percent of 55%) was lower than that in the latter. SBA-15 showed low activity to the oxidation reaction but exhibited good capacity to RhB adsorption. It has been suggested that the good activity of $LaFeO_3$/SBA-15 was majorly attributed to a synergistic effect between $LaFeO_3$ and SBA-15, where $LaFeO_3$ was the active site of the oxidation reaction and SBA-15, besides as a support of $LaFeO_3$, acted as a gallery to adsorb and transport the RhB from solution to the surface of $LaFeO_3$, to guarantee the sufficient supply of RhB to the reaction and accelerate the reaction rate.[41] This was also supported by a later experiment using La−Cu−O/SBA-15 catalyst for investigation, as illustrated in Figure 27.[50] However,

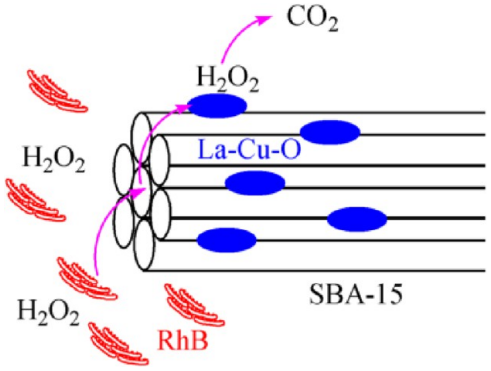

Figure 27. Proposed reaction route for the oxidation of RhB with H_2O_2over La−Cu−O/SBA-15.[50]

it is also possible that the increased surface area (and the more exposed active sites) caused by decreasing the particle size

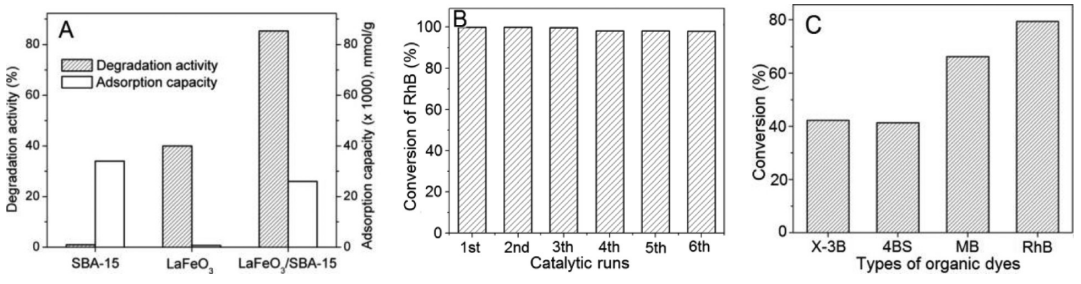

Figure 26. (A) Degradation activity (weight ratio of RhB to catalyst is 0.08, using H_2O_2 as oxidant and the data were obtained at reaction time of 3h) and adsorption capacity of SBA-15, $LaFeO_3$, and $LaFeO_3$/SBA-15 for RhB; (B) Catalytic activity of $LaFeO_3$/SBA-15 for RhB oxidation within six runs; (C) Catalytic activity of $LaFeO_3$/SBA-15 for various organic dyes; For (B) and (C), the weight ratio of RhB to $LaFeO_3$/SBA-15 is 0.0048, and reaction time is 2 h.[41]

dx.doi.org/10.1021/cs500606g | ACS Catal. 2014, 4, 2917−2940

contributed to the reaction. Actually from the role of SBA-15 in the reaction it can be inferred that surface area is very important to the reaction, which offers at least the possibility to absorb more reactants to the active site.

Further studies indicated that the supported perovskite $LaFeO_3$/SBA-15 was highly stable and can be reused for at least six times without appreciable loss in the activity. This material could also be applied to various organic dyes, including Reactive brilliant red X-3B, direct scarlet 4BS and methylene blue (MB), in wide working pH ranges (2−11), Figure 26B,C, pointing out the excellent performances of supported perovskite oxides for liquid-phase degradation of organic dyes.

The above results suggested that the catalytic performances of perovskite oxide for dye oxidation can be optimized by dispersing nanosized particles on porous support as well as synergistic enhancement with the porous support. Small particle size is normally beneficial to catalytic reaction because of its high ratio of surface to bulk atoms, whereas the porous support that possesses high adsorption capacity for substrate could guarantee the sufficient supply of substrate to the active site. The incorporation of them thus offers a new technology for the preparation of active perovskite catalysts used for liquid-phase reactions.

4.10. Application to Other Reactions. Besides the above-mentioned reactions, perovskite oxides are also promising catalysts for various other reactions such as oxidative coupling of methane,[270−272] dehydrogenation of organic substrates,[273−275] hydrogenation of carbon oxides,[276] oxygen evolution,[133] CO_2 reforming of CH_4,[277,278] hydroxylation of phenol,[279] among others. For more information on these applications, we refer the reader to the literature. Another important application of perovskite oxide is for photocatalytic reaction. Although there have been some reports on the application of perovskite oxides for photocatalysis,[17,280−284] the volume is much smaller than that for heterogeneous catalysis. Perovskite oxide in theory should be a suitable photocatalyst as the conduction band and the valence band, which are composed of the 3d orbit of B-site cation and the 2p orbit of oxygen respectively, can be adjusted by substitution with a foreign cation at either A- or B-site, changing the band gap and thus responding to light with different wavelengths. We believe that this application would gain more attention in the future because of the energy deficiency.

5. CONCLUSIONS

We have given a brief survey of the method for preparing perovskite oxides with different morphologies, several common but important means for characterizing perovskite oxides, and the applications of perovskite oxides in heterogeneous catalysis. The perovskite oxides are compounds consisting of several simple oxides and normally have low surface area as the integration of simple oxides requires high temperature and long calcination time. For application in heterogeneous catalysis of reactions on surface, the enhancement of surface area and surface properties for the perovskite oxides are essential. To this end, this review summarized several methods for the preparation of perovskite oxides with different morphologies, including bulk, nanosized, supported, porous, and hollow, which will enhance the surface area and surface properties and satisfy special demand for different reactions. In order to understand the material better, several technologies were introduced to characterize the structure and physicochemical properties of the perovskite oxides. With respect to the applications in heterogeneous catalysis, catalytic performances of perovskite oxides with different morphologies for gas, solid, and liquid-phase reactions have been overviewed. For gaseous reactions carried out at high temperature, the presence of oxygen vacancy is essential, as it is an adsorption and/or active site of the substrate. Meanwhile, the match of redox potentials should be considered. For solid-phase reactions, because of the mobility shortage of the reactant, it is important to increase the surface area in order to enhance the contact area between the catalyst and the solid reactant. For liquid-phase reactions carried out at room temperatures using H_2O_2 as oxidant, the redox couple M^{n+}/M^{n+1} is assumed to be the active site, whereas the oxidation capacity should be controlled to avoid H_2O_2 decomposition before participating in the reaction. The use of supported catalyst would benefit such reactions by minimizing the particle size and with assistance from the porous support.

Although great achievements in academics have been obtained over the years, perovskite oxides have not yet found their application as a commercial catalyst. Partial problems could be due to their low catalytic efficiency and weak resistance to poisons (e.g., sulfur dioxide). Ongoing and future efforts thus should pay much attention to how to prepare a more efficient catalyst and learn the knowledge of the interaction between the poisons and the surface of perovskite oxides in order to commercialize these materials for industrial use.

AUTHOR INFORMATION

Corresponding Authors

*E-mail: (J.Z.) ciaczjj@gmail.com.
*E-mail: (X.Y.) xgyang@ciac.ac.cn.
*E-mail: (Z.Z.) zhenzhao@cup.edu.cn.

Notes

The authors declare no competing financial interest.

ACKNOWLEDGMENTS

We thank gratefully to Prof. Kongyong Liew at South-central University for Nationalities for correcting the English usage. Financial support from the National Science Foundation of China (21203254, 21273221, 21177160, 21177120) and the Scientific Research Foundation for Returned Scholars, Ministry of Education of China (BZY11055) is gratefully acknowledged.

REFERENCES

(1) Zhu, J. J.; Thomas, A. *Appl. Catal., B* **2009**, *92*, 225−233.
(2) Voorhoeve, R. J. H. *Advanced Materials in Catalysis*; Academic Press: New York, 1977.
(3) Pena, M. A.; Fierro, J. L. G. *Chem. Rev.* **2001**, *101*, 1981−2017.
(4) Voorhoeve, R. J. H.; Remeika, J. P.; Trimble, L. E. *Ann. Ny. Acad. Sci.* **1976**, *272*, 3−21.
(5) Goldschmidt, V. M. *Die Naturwissenschaften* **1926**, *21*, 477−485.
(6) Zhu, J. J.; Xiao, D. H.; Li, J.; Yang, X. G.; Wei, K. M. *Catal. Commun.* **2006**, *7*, 432−435.
(7) Xu, J.; Liu, J.; Zhao, Z.; Zheng, J.; Zhang, G.; Duan, A.; Jiang, G. *Catal. Today* **2010**, *153*, 136−142.
(8) Wu-Laitao Luo, Y.; Liu, W. *J. Chem. Sci.* **2007**, *119*, 237−241.
(9) Wang, Y.; Cui, X.; Li, Y.; Shu, Z.; Chen, H.; Shi, J. *Microporous Mesoporous Mater.* **2013**, *176*, 8−15.
(10) Royer, S.; Bérubé, F.; Kaliaguine, S. *Appl. Catal., A* **2005**, *282*, 273−284.
(11) Wang, H.; Zhao, Z.; Liang, P.; Xu, C.; Duan, A.; Jiang, G.; Xu, J.; Liu, J. *Catal. Lett.* **2008**, *124*, 91−99.

(12) Chiarello, G. L.; Grunwaldt, J. D.; Ferri, D.; Krumeich, F.; Oliva, C.; Forni, L.; Baiker, A. *J. Catal.* **2007**, *252*, 127−136.
(13) Kimura, M.; Niwa, Y.; Uemura, K.; Nagai, T.; Inada, Y.; Nomura, M. *Mater. Trans.* **2013**, *54*, 246−254.
(14) Nishihata, Y.; Mizuki, J.; Tanaka, H.; Uenishi, M.; Kimura, M. *J. Phys. Chem. Solids* **2005**, *66*, 274−282.
(15) Parravano, G. *J. Chem. Phys.* **1952**, *20*, 342−343.
(16) Parravano, G. *J. Am. Chem. Soc.* **1953**, *75*, 1497−1498.
(17) Maegli, A. E.; Hisatomi, T.; Otal, E. H.; Yoon, S.; Pokrant, S.; Gratzel, M.; Weidenkaff, A. *J. Mater. Chem.* **2012**, *22*, 17906−17913.
(18) Zhang, H.; Chen, G.; Li, Z.; Liu, J. *J. Rare Earth* **2007**, *25*, 293−296.
(19) Wei, Z.-X.; Wang, Y.; Liu, J.-P.; Xiao, C.-M.; Zeng, W.-W. *Mater. Chem. Phys.* **2012**, *136*, 755−761.
(20) Su, H.; Jing, L.; Shi, K.; Yao, C.; Fu, H. *J. Nanopart. Res.* **2010**, *12*, 967−974.
(21) Chroneos, A.; Vovk, R. V.; Goulatis, I. L.; Goulatis, L. I. *J. Alloy. Compd.* **2010**, *494*, 190−195.
(22) Tejuca, L. G.; Fierro, J. L. G.; Tascon, J. M. D. *Adv. Catal.* **1989**, *36*, 237−328.
(23) Zwinkels, M. F. M.; Järås, S. G.; Menon, P. G.; Griffin, T. A. *Catal. Rev.* **1993**, *35*, 319−358.
(24) Tejuca, L. G.; Fierro, J. L. G.: *Properties and Applications of Perovskite-type Oxides*; CRC Press: New York, 1993.
(25) Lombardo, E. A.; Ulla, M. A. *Res. Chem. Intermed.* **1998**, *24*, 581−592.
(26) Misono, M. *Stud. Surf. Sci. Catal.* **2013**, *176*, 67−95.
(27) Schaak, R. E.; Mallouk, T. E. *Chem. Mater.* **2002**, *14*, 1455−1471.
(28) Ma, W. H.; Xie, G.; Chen, S. R.; Cui, H. *Trans. Nonferrous Met. Soc. China* **2011**, *11*, 904−907.
(29) Bhella, S. S.; Kuti, L. M.; Li, Q.; Thangadurai, V. *Dalton. Trans.* **2009**, 9520−9528.
(30) Isupova, L. A.; Alikina, G. M.; Tsybulya, S. V.; Boldyreva, N. N.; Kryukova, G. N.; Yakovleva, I. S.; Isupov, V. P.; Sadykov, V. A. *Int. J. Inorg. Mater.* **2001**, *3*, 559−562.
(31) Sakamoto, W.; Itoh, N.; Shimura, T.; Yogo, T. *ISAF: Nara* **2007**, 426−427.
(32) Bhalla, A. S.; Guo, R.; Roy, R. *Mater. Res. Innov.* **2000**, *4*, 3−26.
(33) Zhang, S.; Xia, R.; Shrout, T. R.; Zang, G.; Wang, J. *J. Appl. Phys.* **2006**, *100*, 104108.
(34) Zhu, J. J.; Mao, D. H.; Li, J.; Xie, X. F.; Yang, X. G.; Wu, Y. *J. Mol. Catal. A: Chem.* **2005**, *233*, 29−34.
(35) Zhu, J. J.; Yang, X. G.; Xu, X. L.; Wei, K. M. *J. Phys. Chem. C* **2007**, *111*, 1487−1490.
(36) Zhu, J. J.; Zhao, Z.; Xiao, D. H.; Li, J.; Yang, X. G.; Wu, Y. *J. Mol. Catal. A: Chem.* **2005**, *238*, 35−40.
(37) Silva, G.; Santos, J.; Martinelli, D.; Pedrosa, A.; de Souza, M.; Melo, D. *Mater. Sci. Appl.* **2010**, *1*, 39−45.
(38) Zhu, J. J.; Xiao, D. H.; Li, J.; Yang, X. G.; Wu, Y. *J. Mol. Catal. A: Chem.* **2005**, *234*, 99−105.
(39) Wang, N.; Yu, X.; Wang, Y.; Chu, W.; Liu, M. *Catal. Today* **2013**, *212*, 98−107.
(40) Nguyen, S. V.; Szabo, V.; Trong On, D.; Kaliaguine, S. *Microporous Mesoporous Mater.* **2002**, *54*, 51−61.
(41) Xiao, P.; Hong, J.; Wang, T.; Xu, X.; Yuan, Y.; Li, J.; Zhu, J. *Catal. Lett.* **2013**, *143*, 887−894.
(42) Ding, Q.; Xian, H.; Tan, Y.; Tsubaki, N.; Li, X. *Catal. Sci. Technol.* **2013**, *3*, 1493−1496.
(43) Alifanti, M.; Blangenois, N.; Florea, M.; Delmon, B. *Appl. Catal,. A* **2005**, *280*, 255−265.
(44) Zhang, J.; Weng, X.; Wu, Z.; Liu, Y.; Wang, H. *Appl. Catal., B* **2012**, *126*, 231−238.
(45) Chagas, C. A.; Toniolo, F. S.; Magalhães, R. N. S. H.; Schmal, M. *Int. J. Hydrogen. Energ* **2012**, *37*, 5022−5031.
(46) Kathiraser, Y.; Thitsartarn, W.; Sutthiumporn, K.; Kawi, S. *J. Phys. Chem. C* **2013**, *117*, 8120−8130.
(47) Arnone, S.; Busca, G.; Lisi, L.; Milella, F.; Russo, G.; Turco, M. *Symp. (Int.) Combust., [Proc.]* **1998**, *27*, 2293−2299.
(48) Škapin, S.; Kolar, D.; Suvorov, D. *J. Am. Ceram. Soc.* **1993**, *76*, 2359−2362.
(49) Cimino, S.; Pirone, R.; Russo, G. *Ind. Eng. Chem. Res.* **2000**, *40*, 80−85.
(50) Xiao, P.; Li, H.; Wang, T.; Xu, X.; Li, J.; Zhu, J. *RSC Adv.* **2014**, *4*, 12601−12604.
(51) Labhsetwar, N. K.; Watanabe, A.; Biniwale, R. B.; Kumar, R.; Mitsuhashi, T. *Appl. Catal., B* **2001**, *33*, 165−173.
(52) Labhsetwar, N.; Biniwale, R. B.; Kumar, R.; Rayalu, S.; Devotta, S. *Catal. Surv. Asia* **2006**, *10*, 55−64.
(53) Shao, Y.; Wang, X.-F.; Ao, M.; Gong, C.-R.; Fan, G.-L.; Chen, H.-F. *Front. Mater. Sci.* **2012**, *6*, 304−310.
(54) Zhai, Y.; Xiong, J.; Li, C.; Xu, X.; Luo, G. *J. Rare Earth* **2010**, *28*, 54−58.
(55) Wang, G.; Liu, D.; Bing, L. *IEEE* **2011**, 7154−7157.
(56) Cimino, S.; Lisi, L.; Pirone, R.; Russo, G.; Turco, M. *Catal. Today* **2000**, *59*, 19−31.
(57) Algueró, M.; Ricote, J.; Hungría, T.; Castro, A. *Chem. Mater.* **2007**, *19*, 4982−4990.
(58) Moure, A.; Castro, A.; Tartaj, J.; Moure, C. *Ceram. Int.* **2009**, *35*, 2659−2665.
(59) Algueró, M.; Ricote, J.; Castro, A. *J. Am. Ceram. Soc.* **2004**, *87*, 772−778.
(60) Sepelak, V.; Duvel, A.; Wilkening, M.; Becker, K.-D.; Heitjans, P. *Chem. Soc. Rev.* **2013**, *42*, 7507−7520.
(61) James, S. L.; Adams, C. J.; Bolm, C.; Braga, D.; Collier, P.; Friscic, T.; Grepioni, F.; Harris, K. D. M.; Hyett, G.; Jones, W.; Krebs, A.; Mack, J.; Maini, L.; Orpen, A. G.; Parkin, I. P.; Shearouse, W. C.; Steed, J. W.; Waddell, D. C. *Chem. Soc. Rev.* **2012**, *41*, 413−447.
(62) Kaliaguine, S.; Van Neste, A.; Szabo, V.; Gallot, J. E.; Bassir, M.; Muzychuk, R. *Appl. Catal., A* **2001**, *209*, 345−358.
(63) Szabo, V.; Bassir, M.; Van Neste, A.; Kaliaguine, S. *Appl. Catal., B* **2002**, *37*, 175−180.
(64) Szabo, V.; Bassir, M.; Van Neste, A.; Kaliaguine, S. *Appl. Catal., B* **2003**, *43*, 81−92.
(65) Szabo, V.; Bassir, M.; Gallot, J. E.; Van Neste, A.; Kaliaguine, S. *Appl. Catal., B* **2003**, *42*, 265−277.
(66) Yang, W. Controlled synthesis of highly active nanosized LaFe-based perovskites and mechanism study for their catalytic removing small molecule pollution gases. Ph.D. Thesis, Beijing University of Chemical Technology, May 2013.
(67) Perejon, A.; Murafa, N.; Sanchez-Jimenez, P. E.; Criado, J. M.; Subrt, J.; Dianez, M. J.; Perez-Maqueda, L. A. *J. Mater. Chem. C* **2013**, *1*, 3551−3562.
(68) Gao, B.; Deng, J.; Liu, Y.; Zhao, Z.; Li, X.; Wang, Y.; Dai, H. *Chin. J. Catal.* **2013**, *34*, 2223−2229.
(69) Liu, Y.; Dai, H.; Du, Y.; Deng, J.; Zhang, L.; Zhao, Z.; Au, C. T. *J. Catal.* **2012**, *287*, 149−160.
(70) Wang, Y. G.; Ren, J. W.; Wang, Y. Q.; Zhang, F. Y.; Liu, X. H.; Guo, Y.; Lu, G. Z. *J. Phys. Chem. C* **2008**, *112*, 15293−15298.
(71) Civera, A.; Pavese, M.; Saracco, G.; Specchia, V. *Catal. Today* **2003**, *83*, 199−211.
(72) Zou, Z.-Q.; Meng, M.; Luo, J.-Y.; Zha, Y.-Q.; Xie, Y.-N.; Hu, T.-D.; Liu, T. *J. Mol. Catal. A: Chem.* **2006**, *249*, 240−245.
(73) Zhao, Z.; Dai, H.; Deng, J.; Du, Y.; Liu, Y.; Zhang, L. *Microporous Mesoporous Mater.* **2012**, *163*, 131−139.
(74) Sadakane, M.; Asanuma, T.; Kubo, J.; Ueda, W. *Chem. Mater.* **2005**, *17*, 3546−3551.
(75) Xu, J.; Liu, J.; Zhao, Z.; Xu, C.; Zheng, J.; Duan, A.; Jiang, G. *J. Catal.* **2011**, *282*, 1−12.
(76) Xiao, P.; Zhu, J.; Li, H.; Jiang, W.; Wang, T.; Zhu, Y.; Zhao, Y.; Li, J. *ChemCatChem* **2014**, *6*, 1774−1781.
(77) Zhao, D. Y.; Feng, J. L.; Huo, Q. S.; Melosh, N.; Fredrickson, G. H.; Chmelka, B. F.; Stucky, G. D. *Science* **1998**, *279*, 548−552.
(78) Zhu, J.; Kailasam, K.; Xie, X.; Schomaecker, R.; Thomas, A. *Chem. Mater.* **2011**, *23*, 2062−2067.
(79) Zhu, J.; Xie, X.; Carabineiro, S. A. C.; Tavares, P. B.; Figueiredo, J. L.; Schomacker, R.; Thomas, A. *Energy Environ. Sci.* **2011**, *4*, 2020−2024.

(80) Fino, D.; Solaro, S.; Russo, N.; Saracco, G.; Specchia, V. *Top. Catal.* **2007**, *42*−*43*, 449−454.
(81) Specchia, S.; Galletti, C.; Specchia, V. *Stud. Surf. Sci. Catal.* **2010**, *175*, 59−67.
(82) Mukasyan, A. S.; Dinka, P. *Int. J. Self-Propag. High-Temp. Synth.* **2007**, *16*, 23−35.
(83) Zhu, C.; Nobuta, A.; Nakatsugawa, I.; Akiyama, T. *Int. J. Hydrogen Energy* **2013**, *38*, 13238−13248.
(84) Fu, S.; Niu, H.; Tao, Z.; Song, J.; Mao, C.; Zhang, S.; Chen, C.; Wang, D. *J. Alloys Compd.* **2013**, *576*, 5−12.
(85) Ji, K.; Dai, H.; Deng, J.; Zhang, L.; Jiang, H.; Xie, S.; Han, W. *J. Mol. Catal. A: Chem.* **2013**, *370*, 189−196.
(86) Gao, P.; Li, N.; Wang, A.; Wang, X.; Zhang, T. *Mater. Lett.* **2013**, *92*, 173−176.
(87) Kim, Y. N.; Kim, J. C.; Lee, E. K.; Hwang, Y. S.; Hur, N. H.; Yun, Y. J.; Park, G. S.; Kim, J. T. *J. Appl. Phys.* **2004**, *95*, 7088−7090.
(88) Chen, X.; Hu, J.; Chen, Z.; Feng, X.; Li, A. *Biosens. Bioelectron.* **2009**, *24*, 3448−3454.
(89) Li, S.; Nechache, R.; Davalos, I. A. V.; Goupil, G.; Nikolova, L.; Nicklaus, M.; Laverdiere, J.; Ruediger, A.; Rosei, F. *J. Am. Ceram. Soc.* **2013**, *96*, 3155−3162.
(90) Leng, J.; Li, S.; Wang, Z.; Xue, Y.; Xu, D. *Mater. Lett.* **2010**, *64*, 1912−1914.
(91) Li, S.; Kato, R.; Wang, Q.; Yamanaka, T.; Takeguchi, T.; Ueda, W. *Appl. Catal., B* **2010**, *93*, 383−386.
(92) Zhu, X.; Liu, Z.; Ming, N. *J. Mater. Chem.* **2010**, *20*, 4015−4030.
(93) Wang, J.; Manivannan, A.; Wu, N. *Thin Solid Films* **2008**, *517*, 582−587.
(94) Chen, X.; Tang, Y.; Fang, L.; Zhang, H.; Hu, C.; Zhou, H. *J. Mater. Sci.: Mater. Electron.* **2012**, *23*, 1500−1503.
(95) Wang, W.; Bi, J.; Wu, L.; Li, Z.; Fu, X. *Scripta Mater.* **2009**, *60*, 186−189.
(96) Deng, J.; Zhang, L.; Dai, H.; Au, C. *Catal. Lett.* **2009**, *130*, 622−629.
(97) Nakashima, K.; Kera, M.; Fujii, I.; Wada, S. *Ceram. Int.* **2013**, *39*, 3231−3234.
(98) Rao, G. V. S.; Rao, C. N. R.; Ferraro, J. R. *Appl. Spectrosc.* **1970**, *24*, 436−445.
(99) Wu, Y.; Yu, T.; Dou, B. S.; Wang, C. X.; Xie, X. F.; Yu, Z. L.; Fan, S. R.; Fan, Z. R.; Wang, L. C. *J. Catal.* **1989**, *120*, 88−107.
(100) Yu, Z.; Gao, L.; Yuan, S.; Wu, Y. *J. Chem. Soc., Faraday Trans.* **1992**, *88*, 3245−3249.
(101) Gushee, B. E.; Katz, L.; Ward, R. *J. Am. Chem. Soc.* **1957**, *79*, 5601−5603.
(102) Harris, D. C.; Hewston, T. A. *J. Solid State Chem.* **1987**, *69*, 182−185.
(103) Ciambelli, P.; Cimino, S.; De Rossi, S.; Faticanti, M.; Lisi, L.; Minelli, G.; Pettiti, I.; Porta, P.; Russo, G.; Turco, M. *Appl. Catal., B* **2000**, *24*, 243−253.
(104) Yamazoe, N.; Teraoka, Y. *Catal. Today* **1990**, *8*, 175−199.
(105) Fino, D.; Russo, N.; Saracco, G.; Specchia, V. *J. Catal.* **2003**, *217*, 367−375.
(106) Teraoka, Y.; Yoshimatsu, M.; Yamazoe, N.; Seiyama, T. *Chem. Lett.* **1984**, *13*, 893−896.
(107) Rossetti, I.; Forni, L. *Appl. Catal., B* **2001**, *33*, 345−352.
(108) Zhao, Z.; Yang, X. G.; Wu, Y. *Appl. Catal., B* **1996**, *8*, 281−297.
(109) Zhu, J. J.; Xiao, D. H.; Li, J.; Yang, X. G. *Catal. Lett.* **2009**, *129*, 240−246.
(110) Yang, X.; Luo, L.; Zhong, H. *Appl. Catal., A* **2004**, *272*, 299−303.
(111) Ferri, D.; Forni, L. *Appl. Catal., B* **1998**, *16*, 119−126.
(112) Yamazoe, N.; Teraoka, Y.; Seiyama, T. *Chem. Lett.* **1981**, 1767−1770.
(113) Imamura, M.; Matsubayashi, N.; Shimada, H. *J. Phys. Chem. B* **2000**, *104*, 7348−7353.
(114) Li, X.; Chen, C.; Liu, C.; Xian, H.; Guo, L.; Lv, J.; Jiang, Z.; Vernoux, P. *ACS Catal.* **2013**, *3*, 1071−1075.
(115) Arandiyan, H.; Dai, H.; Deng, J.; Liu, Y.; Bai, B.; Wang, Y.; Li, X.; Xie, S.; Li, J. *J. Catal.* **2013**, *307*, 327−339.
(116) Zhao, Z.; Dai, H.; Deng, J.; Du, Y.; Liu, Y.; Zhang, L. *J. Mol. Catal. A: Chem.* **2013**, *366*, 116−125.
(117) Lisi, L.; Bagnasco, G.; Ciambelli, P.; De Rossi, S.; Porta, P.; Russo, G.; Turco, M. *J. Solid State Chem.* **1999**, *146*, 176−183.
(118) Hansen, K. K.; Skou, E. M.; Christensen, H.; Turek, T. *J. Catal.* **2001**, *199*, 132−140.
(119) Dai, H.; He, H.; Li, P.; Gao, L.; Au, C.-T. *Catal. Today* **2004**, *90*, 231−244.
(120) Russo, N.; Fino, D.; Saracco, G.; Specchia, V. *J. Catal.* **2005**, *229*, 459−469.
(121) Patcas, F.; Buciuman, F. C.; Zsako, J. *Thermochim. Acta* **2000**, *360*, 71−76.
(122) Buciuman, F.; Patcas, F.; Zsakó, J. *J. Therm. Anal. Calorim.* **2000**, *61*, 819−825.
(123) Patcas, F. Heterogen katalysierte Gasphasen-Oxidehydrierung von Cyclohexan an Nickeloxid-Trägerkatalysatoren. Ph.D. Thesis, Technische Universitat Chemnitz, March 1998.
(124) Lee, M. J.; Jun, J. H.; Jung, J. S.; Kim, Y. R.; Lee, S. H. *B. Kor. Chem. Soc.* **2005**, *26*, 1591−1596.
(125) Silva, G. R. O.; Santos, J. C.; Martinelli, D. M. H.; Pedrosa, A. M. G.; de Souza, M. J. B.; Melo, D. M. A. *Mater. Sci. Appl.* **2010**, *1*, 39−45.
(126) Sugunan, S.; Meera, V. *React. Kinet. Catal. Lett.* **1997**, *62*, 327−332.
(127) Lima, E.; Villafuerte-Castrejón, M. E.; Saniger, J. M.; Ibarra-Palos, A.; Sánchez-Sánchez, J. E.; Álvarez, L. J. *Solid State Ionics* **2008**, *178*, 1944−1949.
(128) Ashbrook, S. E.; Le Pollès, L.; Gautier, R.; Pickard, C. J.; Walton, I. *Phys. Chem. Chem. Phys.* **2006**, *8*, 3423−3431.
(129) Forni, L.; Oliva, C.; Barzetti, T.; Selli, E.; Ezerets, A. M.; Vishniakov, A. V. *Appl. Catal., B* **1997**, *13*, 35−43.
(130) Cabello, G.; Lillo, L.; Caro, C.; Buono-Core, G. E.; Chornik, B.; Flores, M.; Carrasco, C.; Rodriguez, C. A. *Ceram. Int.* **2014**, *40*, 7761−7768.
(131) Pal, N.; Paul, M.; Bhaumik, A. *Appl. Catal., A* **2011**, *393*, 153−160.
(132) Zhu, J. J.; Zhao, Z.; Xiao, D.; Li, J.; Yang, X. G.; Wu, Y. *Electrochem. Commun.* **2005**, *7*, 58−61.
(133) Grimaud, A.; May, K. J.; Carlton, C. E.; Lee, Y.-L.; Risch, M.; Hong, W. T.; Zhou, J.; Shao-Horn, Y. *Nat. Commun.* **2013**, *4*, 2439.
(134) Leanza, R.; Rossetti, I.; Fabbrini, L.; Oliva, C.; Forni, L. *Appl. Catal., B* **2000**, *28*, 55−64.
(135) Zhang-Steenwinkel, Y.; van der Zande, L. M.; Castricum, H. L.; Bliek, A. *Appl. Catal., B* **2004**, *54*, 93−103.
(136) Shannon, S. L.; Goodwin, J. G. *Chem. Rev.* **1995**, *95*, 677−695.
(137) Bassat, J. M.; Petitjean, M.; Fouletier, J.; Lalanne, C.; Caboche, G.; Mauvy, F.; Grenier, J. C. *Appl. Catal., A* **2005**, *289*, 84−89.
(138) Bosch, H.; Janssen, F. *Catal. Today* **1988**, *2*, 369−521.
(139) Parvulescu, V. I.; Grange, P.; Delmon, B. *Catal. Today* **1998**, *46*, 233−316.
(140) Teraoka, Y.; Harada, T.; Kagawa, S. *J. Chem. Soc., Faraday Trans.* **1998**, *94*, 1887−1891.
(141) Shin, S.; Arakawa, H.; Hatakeyama, Y.; Ogawa, K.; Shimomura, K. *Mater. Res. Bull.* **1979**, *14*, 633−639.
(142) Ishihara, T.; Ando, M.; Sada, K.; Takiishi, K.; Yamada, K.; Nishiguchi, H.; Takita, Y. *J. Catal.* **2003**, *220*, 104−114.
(143) Zhu, Y. J.; Wang, D.; Yuan, F. L.; Zhang, G.; Fu, H. G. *Appl. Catal., B* **2008**, *82*, 255−263.
(144) Deng, J.; Zhang, L.; Xia, Y.; Dai, H.; He, H. *J. Environ. Sci.* **2010**, *22*, 448−453.
(145) Tofan, C.; Klvana, D.; Kirchnerova, J. *Appl. Catal., A* **2002**, *223*, 275−286.
(146) Zhu, J.; Yang, X.; Xu, X.; Wei, K. *Sci. China Ser. B* **2007**, *50*, 41−46.
(147) Yasuda, H.; Mizuno, N.; Misono, M. *J. Chem. Soc., Chem. Commun.* **1990**, 1094−1096.
(148) Belessi, V. C.; Trikalitis, P. N.; Ladavos, A. K.; Bakas, T. V.; Pomonis, P. J. *Appl. Catal., A* **1999**, *177*, 53−68.

(149) Zhu, J. J.; Zhao, Z.; Xiao, D. H.; Li, J.; Yang, X. G.; Wu, Y. *Ind. Eng. Chem. Res.* **2005**, *44*, 4227−4233.
(150) Viswanathan, B. *Catal. Rev.* **1992**, *34*, 337−354.
(151) Khristova, M.; Petrović, S.; Terlecki-Baričević, A.; Mehandjiev, D. *Cent. Eur. J. Chem.* **2009**, *7*, 857−863.
(152) Zhang, R.; Luo, N.; Yang, W.; Liu, N.; Chen, B. *J. Mol. Catal. A: Chem.* **2013**, *371*, 86−93.
(153) Zhang, Y.; Wang, D.; Wang, J.; Chen, Q.; Zhang, Z.; Pan, X.; Miao, Z.; Zhang, B.; Wu, Z.; Yang, X. *Chin. J. Catal.* **2012**, *33*, 1448−1454.
(154) Zhang, R.; Yang, W.; Luo, N.; Li, P.; Lei, Z.; Chen, B. *Appl. Catal., B* **2014**, *146*, 94−104.
(155) Yang, W.; Zhang, R.; Chen, B.; Duprez, D.; Royer, S. *Environ. Sci. Technol.* **2012**, *46*, 11280−11288.
(156) Furfori, S.; Russo, N.; Fino, D.; Saracco, G.; Specchia, V. *Chem. Eng. Sci.* **2010**, *65*, 120−127.
(157) Costa, C. N.; Stathopoulos, V. N.; Belessi, V. C.; Efstathiou, A. M. *J. Catal.* **2001**, *197*, 350−364.
(158) Bensaid, S.; Borla, E. M.; Russo, N.; Fino, D.; Specchia, V. *Ind. Eng. Chem. Res.* **2010**, *49*, 10323−10333.
(159) Ferri, D.; Forni, L.; Dekkers, M. A. P.; Nieuwenhuys, B. E. *Appl. Catal., B* **1998**, *16*, 339−345.
(160) Liu, Z.; Li, J.; Woo, S. I. *Energy Environ. Sci.* **2012**, *5*, 8799−8814.
(161) Giannakas, A. E.; Ladavos, A. K.; Pomonis, P. J. *Appl. Catal., B* **2004**, *49*, 147−158.
(162) Zhang, R.; Alamdari, H.; Kaliaguine, S. *J. Catal.* **2006**, *242*, 241−253.
(163) Nishihata, Y.; Mizuki, J.; Akao, T.; Tanaka, H.; Uenishi, M.; Kimura, M.; Okamoto, T.; Hamada, N. *Nature* **2002**, *418*, 164−167.
(164) Taniguchi, M.; Tanaka, H.; Uenishi, M.; Tan, I.; Nishihata, Y.; Mizuki, J. i.; Suzuki, H.; Narita, K.; Hirai, A.; Kimura, M. *Top. Catal.* **2007**, *42*−*43*, 367−371.
(165) Tanaka, H.; Taniguchi, M.; Uenishi, M.; Kajita, N.; Tan, I.; Nishihata, Y.; Mizuki, J. i.; Narita, K.; Kimura, M.; Kaneko, K. *Angew. Chem., Int. Ed.* **2006**, *45*, 5998−6002.
(166) Uenishi, M.; Taniguchi, M.; Tanaka, H.; Kimura, M.; Nishihata, Y.; Mizuki, J.; Kobayashi, T. *Appl. Catal., B* **2005**, *57*, 267−273.
(167) Tian, Z.-x.; Uozumi, A.; Hamada, I.; Yanagisawa, S.; Kizaki, H.; Inagaki, K.; Morikawa, Y. *Nanoscale Res. Lett.* **2013**, *8*, 1−7.
(168) Yanagisawa, S.; Takeda, A.; Inagaki, K.; Hamada, I.; Morikawa, Y. *Catal. Lett.* **2014**, *144*, 736−743.
(169) Guo, X.; Meng, M.; Dai, F.; Li, Q.; Zhang, Z.; Jiang, Z.; Zhang, S.; Huang, Y. *Appl. Catal., B* **2013**, *142*−*143*, 278−289.
(170) Voorhoeve, R. J. H.; Remeika, J. P.; Trimble, L. E.; Cooper, A. S.; Disalvo, F. J.; Gallagher, P. K. *J. Solid State Chem.* **1975**, *14*, 395−406.
(171) Kim, C. H.; Qi, G.; Dahlberg, K.; Li, W. *Science* **2010**, *327*, 1624−1627.
(172) Wang, W.; McCool, G.; Kapur, N.; Yuan, G.; Shan, B.; Nguyen, M.; Graham, U. M.; Davis, B. H.; Jacobs, G.; Cho, K.; Hao, X. *Science* **2012**, *337*, 832−835.
(173) Chen, J.; Shen, M.; Wang, X.; Qi, G.; Wang, J.; Li, W. *Appl. Catal., B* **2013**, *134*−*135*, 251−257.
(174) Chen, J.; Shen, M.; Wang, X.; Wang, J.; Su, Y.; Zhao, Z. *Catal. Commun.* **2013**, *37*, 105−108.
(175) Constantinou, C.; Li, W.; Qi, G.; Epling, W. S. *Appl. Catal., B* **2013**, *134*−*135*, 66−74.
(176) Dong, Y.-H.; Xian, H.; Lv, J.-L.; Liu, C.; Guo, L.; Meng, M.; Tan, Y.-S.; Tsubaki, N.; Li, X.-G. *Mater. Chem. Phys.* **2014**, *143*, 578−586.
(177) Say, Z.; Dogac, M.; Vovk, E. I.; Kalay, Y. E.; Kim, C. H.; Li, W.; Ozensoy, E. *Appl. Catal., B* **2014**, *154*−*155*, 51−61.
(178) Després, J.; Elsener, M.; Koebel, M.; Kröcher, O.; Schnyder, B.; Wokaun, A. *Appl. Catal., B* **2004**, *50*, 73−82.
(179) Bourges, P.; Lunati, S.; Mabilon, G. *Stud. Surf. Sci. Catal.* **1998**, *116*, 213−222.
(180) Kramlich, J. C.; Linak, W. P. *Prog. Energy Combust. Sci.* **1994**, *20*, 149−202.
(181) Wójtowicz, M. A.; Pels, J. R.; Moulijn, J. A. *Fuel Process. Technol.* **1993**, *34*, 1−71.
(182) Granger, P.; Parvulescu, V. I. *Chem. Rev.* **2011**, *111*, 3155−3207.
(183) Pérez-Ramírez, J.; Kapteijn, F.; Schöffel, K.; Moulijn, J. A. *Appl. Catal., B* **2003**, *44*, 117−151.
(184) Kapteijn, F.; Rodriguez-Mirasol, J.; Moulijn, J. A. *Appl. Catal., B* **1996**, *9*, 25−64.
(185) Reddy, P. S. S.; Pasha, N.; Chalapathi Rao, M. G. V.; Lingaiah, N.; Suryanarayana, I.; Sai Prasad, P. S. *Catal. Commun.* **2007**, *8*, 1406−1410.
(186) Burch, R.; Daniells, S. T.; Breen, J. P.; Hu, P. *J. Catal.* **2004**, *224*, 252−260.
(187) Kondratenko, E. V.; Kondratenko, V. A.; Santiago, M.; Pérez-Ramírez, J. *J. Catal.* **2008**, *256*, 248−258.
(188) Pieterse, J. A. Z.; Booneveld, S.; van den Brink, R. W. *Appl. Catal., B* **2004**, *51*, 215−228.
(189) Perez-Ramirez, J.; Kapteijn, F.; Mul, G.; Moulijn, J. A. *Chem. Commun.* **2001**, 693−694.
(190) Pérez-Ramírez, J.; Kapteijn, F.; Mul, G.; Xu, X.; Moulijn, J. A. *Catal. Today* **2002**, *76*, 55−74.
(191) Jiang, H.; Wang, H.; Liang, F.; Werth, S.; Schiestel, T.; Caro, J. *Angew. Chem., Int. Ed.* **2009**, *48*, 2983−2986.
(192) Gunasekaran, N.; Rajadurai, S.; Carberry, J. J. *Catal. Lett.* **1995**, *35*, 373−382.
(193) Kumar, S.; Teraoka, Y.; Joshi, A. G.; Rayalu, S.; Labhsetwar, N. *J. Mol. Catal. A: Chem.* **2011**, *348*, 42−54.
(194) Swamy, C. S.; Christopher, J. *Catal. Rev.* **1992**, *34*, 409−425.
(195) Kumar, S.; Vinu, A.; Subrt, J.; Bakardjieva, S.; Rayalu, S.; Teraoka, Y.; Labhsetwar, N. *Catal. Today* **2012**, *198*, 125−132.
(196) Wu, Y.; Ni, X.; Beaurain, A.; Dujardin, C.; Granger, P. *Appl. Catal., B* **2012**, *125*, 149−157.
(197) Russo, N.; Mescia, D.; Fino, D.; Saracco, G.; Specchia, V. *Ind. Eng. Chem. Res.* **2007**, *46*, 4226−4231.
(198) Dacquin, J. P.; Lancelot, C.; Dujardin, C.; Da Costa, P.; Djega-Mariadassou, G.; Beaunier, P.; Kaliaguine, S.; Vaudreuil, S.; Royer, S.; Granger, P. *Appl. Catal., B* **2009**, *91*, 596−604.
(199) Wu, Y.; Cordier, C.; Berrier, E.; Nuns, N.; Dujardin, C.; Granger, P. *Appl. Catal., B* **2013**, *140*−*141*, 151−163.
(200) Wu, Y.; Dujardin, C.; Granger, P.; Tiseanu, C.; Sandu, S.; Kuncser, V.; Parvulescu, V. I. *J. Phys. Chem. C* **2013**, *117*, 13989−13999.
(201) Dacquin, J. P.; Cabié, M.; Henry, C. R.; Lancelot, C.; Dujardin, C.; Raouf, S. R.; Granger, P. *J. Catal.* **2010**, *270*, 299−309.
(202) Ladavos, A. K.; Pomonis, P. J. *Appl. Catal., A* **1997**, *165*, 73−85.
(203) Zhu, J. J.; Yang, X. G.; Xu, X. L.; Wei, K. M. *Z. Phys. Chem.* **2006**, *220*, 1589−1594.
(204) Zhu, J. J.; Zhao, Z.; Xiao, D. H.; Li, J.; Yang, X. G.; Wu, Y. *Z. Phys. Chem.* **2005**, *219*, 807−815.
(205) Falcon, H.; Martinez-Lope, M. J.; Alonso, J. A.; Fierro, J. L. G. *Appl. Catal., B* **2000**, *26*, 131−142.
(206) Tabata, K.; Matsumoto, I.; Kohiki, S. *J. Mater. Sci.* **1987**, *22*, 1882−1886.
(207) Ciambelli, P.; Cimino, S.; Lasorella, G.; Lisi, L.; De Rossi, S.; Faticanti, M.; Minelli, G.; Porta, P. *Appl. Catal., B* **2002**, *37*, 231−241.
(208) Yan, X.; Huang, Q.; Li, B.; Xu, X.; Chen, Y.; Zhu, S.; Shen, S. *J. Ind. Eng. Chem.* **2013**, *19*, 561−565.
(209) Singh, U. G.; Li, J.; Bennett, J. W.; Rappe, A. M.; Seshadri, R.; Scott, S. L. *J. Catal.* **2007**, *249*, 349−358.
(210) Taguchi, H.; Yamasaki, S.; Itadani, A.; Yosinaga, M.; Hirota, K. *Catal. Commun.* **2008**, *9*, 1913−1915.
(211) Yang, W.; Zhang, R.; Chen, B.; Bion, N.; Duprez, D.; Royer, S. *J. Catal.* **2012**, *295*, 45−58.
(212) Marchetti, L.; Forni, L. *Appl. Catal., B* **1998**, *15*, 179−187.
(213) Specchia, S.; Tacchino, S.; Specchia, V. *Chem. Eng. J.* **2011**, *167*, 622−633.

(214) Taguchi, H.; Matsu-ura, K.; Takada, M.; Hirota, K. *J. Solid State Chem.* **2012**, *190*, 157−161.
(215) Goud, S. K.; Whittenberger, W. A.; Chattopadhyay, S.; Abraham, M. A. *Int. J. Hydrogen Energy* **2011**, *32*, 2868−2874.
(216) Clarke, S. H.; Dicks, A. L.; Pointon, K.; Smith, T. A.; Swann, A. *Catal. Today* **1997**, *38*, 411−423.
(217) J.R, R.-N. *J. Catal.* **1973**, *31*, 173−199.
(218) Brown, L. F. *Int. J. Hydrogen Energy* **2001**, *26*, 381−397.
(219) Slagtern, Å.; Olsbye, U. *Appl. Catal., A* **1994**, *110*, 99−108.
(220) Morales, M.; Espiell, F.; Segarra, M. *Int. J. Hydrogen Energy* **2014**, *39*, 6454−6461.
(221) Vella, L. D.; Villoria, J. A.; Specchia, S.; Mota, N.; Fierro, J. L. G.; Specchia, V. *Catal. Today* **2011**, *171*, 84−96.
(222) Khine, M. S. S.; Chen, L.; Zhang, S.; Lin, J.; Jiang, S. P. *Int. J. Hydrogen Energy* **2013**, *38*, 13300−13308.
(223) Toniolo, F. S.; Magalhães, R. N. S. H.; Perez, C. A. C.; Schmal, M. *Appl. Catal., B* **2012**, *117−118*, 156−166.
(224) Nguyen, T. H.; Łamacz, A.; Beaunier, P.; Czajkowska, S.; Domański, M.; Krztoń, A.; Van Le, T.; Djéga-Mariadassou, G. *Appl. Catal., B* **2014**, *152−153*, 360−369.
(225) Wei, H. J.; Cao, Y.; Ji, W. J.; Au, C. T. *Catal. Commun.* **2008**, *9*, 2509−2514.
(226) Villoria, J. A.; Alvarez-Galvan, M. C.; Al-Zahrani, S. M.; Palmisano, P.; Specchia, S.; specchia, V.; Fierro, J. L. G.; Navarro, R. M. *Appl. Catal., B* **2011**, *105*, 276−288.
(227) Atkinson, R. *Atmos. Environ.* **2000**, *34*, 2063−2101.
(228) Chen, H. L.; Lee, H. M.; Chen, S. H.; Chang, M. B.; Yu, S. J.; Li, S. N. *Environ. Sci. Technol.* **2009**, *43*, 2216−2227.
(229) Fenger, J. *Atmos. Environ.* **2009**, *43*, 13−22.
(230) Blasin-Aubé, V.; Belkouch, J.; Monceaux, L. *Appl. Catal., B* **2003**, *43*, 175−186.
(231) Huang, H.; Liu, Y.; Tang, W.; Chen, Y. *Catal. Commun.* **2008**, *9*, 55−59.
(232) Li, W. B.; Wang, J. X.; Gong, H. *Catal. Today* **2009**, *148*, 81−87.
(233) Pecchi, G.; Reyes, P.; Zamora, R.; Cadús, L. E.; Fierro, J. L. G. *J. Solid State Chem.* **2008**, *181*, 905−912.
(234) Spinicci, R.; Faticanti, M.; Marini, P.; De Rossi, S.; Porta, P. *J. Mol. Catal. A: Chem.* **2003**, *197*, 147−155.
(235) Zhang, C.; Guo, Y.; Guo, Y.; Lu, G.; Boreave, A.; Retailleau, L.; Baylet, A.; Giroir-Fendler, A. *Appl. Catal., B* **2014**, *148−149*, 490−498.
(236) Zhang, C.; Hua, W.; Wang, C.; Guo, Y.; Guo, Y.; Lu, G.; Baylet, A.; Giroir-Fendler, A. *Appl. Catal., B* **2013**, *134−135*, 310−315.
(237) Enterkin, J. A.; Setthapun, W.; Elam, J. W.; Christensen, S. T.; Rabuffetti, F. A.; Marks, L. D.; Stair, P. C.; Poeppelmeier, K. R.; Marshall, C. L. *ACS Catal.* **2011**, *1*, 629−635.
(238) Hosseini, S. A.; Sadeghi, M. T.; Alemi, A.; Niaei, A.; Salari, D.; Kafi-Ahmadi, L. *Chin. J. Catal.* **2010**, *31*, 747−750.
(239) Tichenor, B. A.; Palazzolo, M. A. *Environ. Prog.* **1987**, *6*, 172−176.
(240) Hermia, J.; Vigneron, S. *Catal. Today* **1993**, *17*, 349−358.
(241) Liu, Y.; Dai, H.; Du, Y.; Deng, J.; Zhang, L.; Zhao, Z. *Appl. Catal., B* **2012**, *119−120*, 20−31.
(242) Teraoka, Y.; Nakano, K.; Kagawa, S.; Shangguan, W. F. *Appl. Catal., B* **1995**, *5*, L181−L185.
(243) Teraoka, Y.; Kanada, K.; Kagawa, S. *Appl. Catal., B* **2001**, *34*, 73−78.
(244) Wang, H.; Zhao, Z.; Xu, C.-m.; Liu, J. *Catal. Lett.* **2005**, *102*, 251−256.
(245) Wang, H.; Liu, J.; Zhao, Z.; Wei, Y.; Xu, C. *Catal. Today* **2012**, *184*, 288−300.
(246) Wei, Y.; Liu, J.; Zhao, Z.; Chen, Y.; Xu, C.; Duan, A.; Jiang, G.; He, H. *Angew. Chem., Int. Ed.* **2011**, *50*, 2326−229.
(247) Mescia, D.; Caroca, J. C.; Russo, N.; Labhsetwar, N.; Fino, D.; Saracco, G.; Specchia, V. *Catal. Today* **2008**, *137*, 300−305.
(248) Russo, N.; Furfori, S.; Fino, D.; Saracco, G.; Specchia, V. *Appl. Catal., B* **2008**, *83*, 85−95.
(249) Russo, N.; Fino, D.; Saracco, G.; Specchia, V. *Catal. Today* **2008**, *137*, 306−311.
(250) López-Suárez, F. E.; Bueno-López, A.; Illán-Gómez, M. J.; Adamski, A.; Ura, B.; Trawczynski, J. *Environ. Sci. Technol.* **2008**, *42*, 7670−7675.
(251) Mishra, A.; Prasad, R. *Catal. Rev.* **2014**, *56*, 57−81.
(252) Dhakad, M.; Rayalu, S. S.; Kumar, R.; Doggali, P.; Bakardjieva, S.; Subrt, J.; Mitsuhashi, T.; Haneda, H.; Labhsetwar, N. *Catal. Lett.* **2008**, *121*, 137−143.
(253) Thi Hoang Yen, Q.; Thi Minh Nguyet, T.; Que Chi, T.; Quoc Trung, N.; Thi Toan, N.; Dang Khuong, L. *Adv. Nat. Sci.: Nanosci. Nanotechnol.* **2011**, *2*, 045007.
(254) Zhang, R.; Yang, W.; Xue, J.; Chen, B. *Catal. Lett.* **2009**, *132*, 10−15.
(255) Wang, X.; Qi, X.; Jiang, L.; Chen, Z.; Wang, R.; Wei, K. *J. Phys. Chem. C* **2014**, *118*, 13743−13751.
(256) Kumar, S.; Teraoka, Y.; Joshi, A. G.; Rayalu, S.; Labhsetwar, N. *J. Mol. Catal. A: Chem.* **2011**, *348*, 42−54.
(257) Gu, T. K.; Zhu, R. S.; Ouyang, F. *Adv. Mater. Res.* **2012**, *428*, 61−64.
(258) Zhang, R.; Alamdari, H.; Kaliaguine, S. *Appl. Catal., A* **2008**, *340*, 140−151.
(259) Alifanti, M.; Auer, R.; Kirchnerova, J.; Thyrion, F.; Grange, P.; Delmon, B. *Appl. Catal., B* **2003**, *41*, 71−82.
(260) Zhang-Steenwinkel, Y.; Castricum, H. L.; Beckers, J.; Eiser, E.; Bliek, A. *J. Catal.* **2004**, *221*, 523−531.
(261) Rossetti, I.; Buchneva, O.; Biffi, C.; Rizza, R. *Appl. Catal., B* **2009**, *89*, 383−390.
(262) Tzimpilis, E.; Moschoudis, N.; Stoukides, M.; Bekiaroglou, P. *Appl. Catal., B* **2009**, *87*, 9−17.
(263) Liotta, L. F.; Di Carlo, G.; Pantaleo, G.; Garrido, J. C. H.; Venezia, A. M. *Top. Catal.* **2012**, *55*, 782−791.
(264) Haber, F.; Weiss, J. *Proc. R. Soc. A* **1934**, *147*, 332−351.
(265) Meriç, S.; Selcuk, H.; Gallo, M.; Belgiorno, V. *Desalination* **2005**, *173*, 239−248.
(266) Luo, W.; Zhu, L.; Wang, N.; Tang, H.; Cao, M.; She, Y. *Environ. Sci. Technol.* **2010**, *44*, 1786−1791.
(267) Zhang, L.; Nie, Y.; Hu, C.; Qu, J. *Appl. Catal., B* **2012**, *125*, 418−424.
(268) Wang, N.; Zhu, L.; Lei, M.; She, Y.; Cao, M.; Tang, H. *ACS Catal.* **2011**, *1*, 1193−1202.
(269) Rusevova, K.; Köferstein, R.; Rosell, M.; Richnow, H. H.; Kopinke, F.-D.; Georgi, A. *Chem. Eng. J.* **2014**, *239*, 322−331.
(270) ten Elshof, J. E.; Bouwmeester, H. J. M.; Verweij, H. *Appl. Catal., A* **1995**, *130*, 195−212.
(271) Zeng, Y.; Lin, Y. S.; Swartz, S. L. *J. Membr. Sci.* **1998**, *150*, 87−98.
(272) Xu, S. J.; Thomson, W. J. *AIChE J.* **1997**, *43*, 2731−2740.
(273) Rodriguez-Ramos, I.; Guerrero-Ruiz, A.; Rojas, J. L. G.; Fierro, M. L. *Appl. Catal.* **1991**, *68*, 217−228.
(274) Yi, G.; Hayakawa, T.; Andersen, A.; Suzuki, K.; Hamakawa, S.; York, A. E.; Shimizu, M.; Takehira, K. *Catal. Lett.* **1996**, *38*, 189−195.
(275) Watanabe, R.; Hondo, Y.; Mukawa, K.; Fukuhara, C.; Kikuchi, E.; Sekine, Y. *J. Mol. Catal. A: Chem.* **2013**, *377*, 74−84.
(276) Fierro, J. L. G. *Catal. Rev.* **1992**, *34*, 321−336.
(277) Bhavani, A. G.; Kim, W. Y.; Lee, J. S. *ACS Catal.* **2013**, *3*, 1537−1544.
(278) Xie, X.; Otremba, T.; Littlewood, P.; Schomäcker, R.; Thomas, A. *ACS Catal.* **2012**, *3*, 224−229.
(279) Liu, C.; Zhao, Z.; Yang, X.; Ye, X.; Wu, Y. *Chem. Commun.* **1996**, *0*, 1019−1020.
(280) Li, D.; Zheng, J.; Zou, Z. *J. Phys. Chem. Solids* **2006**, *67*, 801−806.
(281) Pokrant, S.; Maegli, A. E.; Chiarello, G. L.; Weidenkaff, A. *CHIMIA Int. J. Chem.* **2013**, *67*, 162−167.
(282) Boltersdorf, J.; Maggard, P. A. *ACS Catal.* **2013**, *3*, 2547−2555.
(283) Maeda, K.; Lu, D.; Domen, K. *ACS Catal.* **2013**, *3*, 1026−1033.
(284) Phivilay, S. P.; Puretzky, A. A.; Domen, K.; Wachs, I. E. *ACS Catal.* **2013**, *3*, 2920−2929.